UNIVERSITY OF COPENHAGEN
FACULTY OF SCIENCE

Continuous flow analysis of the Dye 3 ice core:

New data from old ice

Margaret Mallory Harlan
(tzb468)

Master's thesis
M.Sc. Climate Change
Submitted: June 29, 2020

Supervisors:
Helle Astrid Kjær and Anders Svensson

Abstract

The Dye 3 ice core was drilled to bedrock in Southern Greenland (65°11'N, 43°50'W) in 1979-1981. The southern Greenland location is characterized by relatively warm temperatures and high accumulation rates. Since its drilling, numerous analyses of the core have been performed, and the ice has since been in freezer storage both in the USA and in Denmark. In October and November 2019, remaining Dye 3 ice, was melted during a continuous flow analysis (CFA) campaign at the Physics of Ice, Climate, and Earth (PICE) section of the Niels Bohr Institute at the University of Copenhagen.

The resulting data covers approximate depths of 1753 to 1820 meters and 1865 to 1918 meters, representing the early Holocene and Glacial Transition and a section of the Last Glacial Period (Greenland Stadials 5-12) respectively. The measured data consist of records of the chemistry and impurities contained in the ice. The chemistry measurements considered in this project include NH_4^+, Ca^{2+}, and pH. Calcium and Ammonium provide information about continental dust and forest fires, respectively, and acidity aids in the identification of volcanic events contained in the core. Additionally, an Abakus laser particle counter was used to determine the quantity and grain size distribution of insoluble particles.

A high-resolution CFA record of the chemistry and impurity measurements of the Dye3 ice core is presented, with a particular focus on the concentration and size distribution of dust and other insoluble particles. The new Dye 3 record is also compared with previous measurements of Dye 3 (Steffensen, 1995), as well as CFA records from the NEEM and NGRIP ice cores (Ruth et al., 2003; Bigler, 2004; Schüpbach et al., 2018). Possible techniques making use of the particle size distribution in investigating volcanic and tephra layers in the ice are presented.

Acknowledgements

Thanks must first go to my advisors, Helle Astrid Kjær, for connecting me with the Dye 3 campaign, introducing me to the CFA work at PICE, and supporting me these past ten months - through the melt campaign, her maternity leave, and even a global pandemic, and Anders Svensson, who graciously "adopted" me as an advisee, supporting me through meetings in person as well as countless emails and video calls throughout the pandemic shutdown. Also to Paul Vallelonga, for patient guidance in the lab, fixing problems as they arose and begrudgingly tolerating our questionable music choices.

I couldn't have asked for a better desk-mate and collaborator than Aylin De Campo - thank you for helping me make sense of all of this data and dissecting line after line of MATLAB code. And to Team CFA, for making 6 weeks of long days in the lab fly by, for celebrating the big and small successes throughout, and for never passing up the opportunity for cake; I am grateful to have shared the lab with you all. Gratitude also goes to my fellow students, office mates, and friends, for consistent moral support and exciting lunchtime discussions. Thanks also to Jenna McGee for kindly offering proofreading help.

I owe thanks also to Sune Rasmussen and Trevor Popp, whose paleoclimatology course at DIS allowed me to walk on the Greenland Ice sheet, first sparked my fascination with ice cores, and inspired me to pursue a degree in Climate Change at the University of Copenhagen. Thanks as well to Tobias Erhardt and Camilla Jensen for the great opportunity to join the 2020 EastGRIP CFA campaign in Bern, Switzerland, and to Iben Koldtoft and Thomas Blunier (among others) for helping to make sure I got home to Copenhagen safely amidst the pandemic border closures.

Finally, to my family, for supporting me in my decision to move to Denmark and always encouraging me to follow my interests wherever they may lead - thank you.

Contents

List of Figures

List of Tables

Preface

Sometimes, when people ask me what I do, or what I study, I am tempted to tell them that I am a time traveler. I picture the confused looks or the chuckle of disbelief, but in reality, I often feel like it's the most accurate, and certainly most evocative, description of paleoclimatology. The ultimate goal of paleoclimatology is to understand what has happened in the past, and what better way to do so than to see, touch, and analyze something that was forged by nature tens, and even hundreds, of thousands of years ago. That something, of course, in this case, is ice. The ice sheets, ice caps, and glaciers of the earth are made up of layer upon layer upon layer of snow that has fallen, year after year, accumulating, and becoming "squozen" (squeezed and frozen – a favorite term of Sune Rasmussen) into ice. This layer cake, this pancake stack of old snow, traps gases and microparticles, tiny traces of the world as it existed when the snow fell. It is these tiny traces, often invisible to the naked eye, that take center stage, allowing paleoclimatologists to glimpse into the past, to become time travelers.

1. Introduction

1.1 Greenland

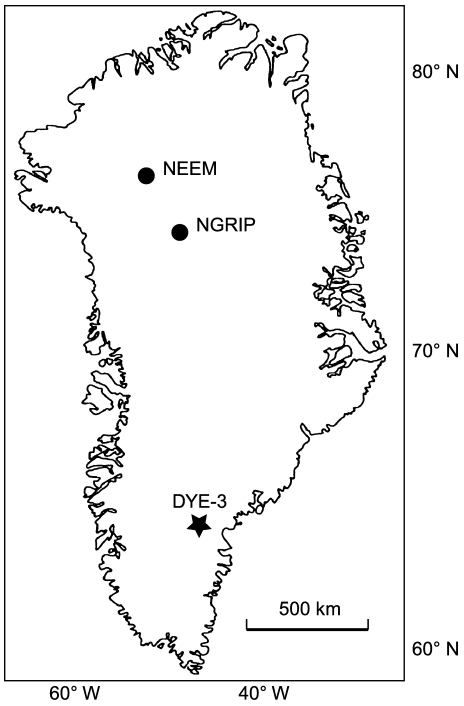

Figure 1. Map of Greenland showing the position of the Dye 3 drilling site, in addition to NEEM and NGRIP (modified from Yau et al. (2016)).

Kalaallit Nunaat, the Kalaallisut name for present day Greenland, has been the home and ancestral land of native Inuit peoples for thousands of years. The island has been inhabited long before colonization by European settlers and continues to be home to over 55,000 people. The largest island in the world, the cold climate of Greenland's interior has allowed for the accumulation of the Greenland Ice Sheet, which covers the majority of Greenland, an area of approximately 1.7 million square kilometers. 3000 meters thick at the thickest point, the consistent accumulation of snow, compressed into ice, on the Greenland Ice Sheet contains ice dating to before the last glacial period, at least 120,000 years b2k. It is this, among other things, that makes Greenland and the Greenland Ice Sheet so important to paleoclimatology and the study of climate change.

To visit Greenland and to walk on the ice sheet is an experience that brings a sense of wonder at the place, the natural world, and the endless potential for learning locked within the ice. The Greenland Ice Sheet has been host to the drilling of at least 8 major deep ice core projects, and countless other scientific

expeditions. Greenland is, however a place that existed before the quest to understand the natural world and climate change and is home to people and animals that are incredibly vulnerable to the impacts of anthropogenic climate change – rising temperatures, thinning sea ice, and shrinking ice sheet, to name just a few. The Greenland Ice Sheet lost over 3,000 billion tons of ice during my lifetime alone due to man-made climate change, causing a mean global sea level rise of over one centimeter (Shepherd et al., 2020).

Scientific field work, even in the field of climate change study, is not exempt from culpability in contributing to increasing emissions, and field work in remote locations like Greenland necessitate significant amounts of air transportation and fuel use. While I believe it is crucial to understand the natural world in an effort to understand the changing climate, it is also important to acknowledge the role of scientists in contributing to it.

1.2 Dye 3

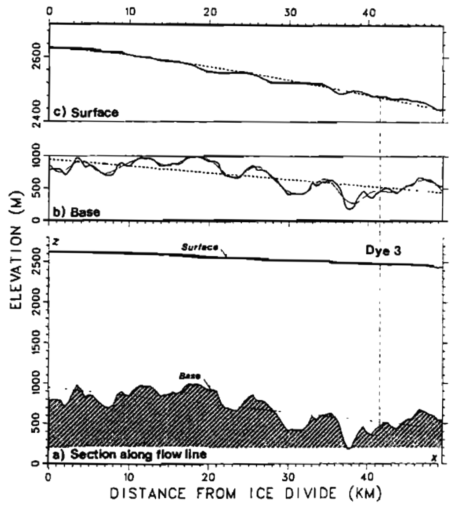

Figure 2. Diagram showing the surface and basal elevation profile of Dye 3 along the flow line from the ice divide. Solid lines represent observed profile. Dye 3 drill site is indicated by a vertical dashed line (reproduced from Reeh, Johnsen, and Dahl-Jensen (1985))

The Dye 3 deep ice core is the primary source of data for this project. It was drilled to a depth of 2037m during the period 1978-1981 at the Dye 3 radar station in southern Greenland (Figure 1, 65°11'N 43°49'W). The site was used for the first deep ice core of the joint Danish, Swiss, and American Greenland Ice Sheet Project (GISP), however due to the Southern Greenland location, distance from the ice divide, and uneven bedrock conditions (Figure 2), Dye 3 was not ideal

for scientific purposes. Finances and logistics, however, led the project to settle on Dye 3 due to the existence of the Dye 3 radar station, despite the fact that it failed to meet almost every one of the predetermined characteristics for a scientifically ideal drill site (Dansgaard et al., 1982; Dansgaard, 2004). A part of the American DEW-line (Distant Early Warning) chain of Cold War radar stations across the Arctic, Dye 3 provided existing workshops, camp housing, and infrastructure, making drilling at that site relatively inexpensive and accessible at the time (Legrand & Mayewski, 1997; Dansgaard, 2004; Langway Jr., 2008).

The ice from Dye 3 has been archived in storage since its drilling in 1981, moving between storage facilities in the US and Denmark as funding schemes changed. Throughout the nearly 40 years since its drilling, it has served as a key source for ice core studies in the intervening time, an important climate archive from the early days of Greenland deep ice core drilling due to its unique location and position in the history of ice core paleoclimatology.

1982 saw the publication of a detailed δ^{18}O record from the Dye 3 ice core, which provided both a high quality record and a comparison to the Camp Century core from Northern Greenland (Dansgaard et al., 1982). More studies into Dye 3 were published in 1985 in *Geophysical Monograph Series 33*, a culmination of many of the GISP efforts thus far. Hammer et al. (1985) present a continuous analysis of impurities for the length of Dye 3 using a modified soldering iron to melt a channel along the cleaned length of the core, continuously pumping out the meltwater for measurements with between 2.5 and 10cm resolution, depending on the impurity measured. This record produced a high resolution data set of dust concentrations as well as electrical conductivity measurements, a newly developed technique used to measure acidity (Neftel et al., 1985). Using these techniques, a correlation was seen between the increased dustiness and alkalinity in the glacial ice and, which was related to the presence of calcium carbonate based material in the ice neutralizing the strong acids present, and additionally dampening the signals of volcanic events during the Last Glacial Period (Hammer et al., 1985).

Also published in 1985 were the results of many other studies based on Dye 3, including ion chromatography results of chloride, nitrate, and sulfate (Herron & Langway Jr., 1985); mechanical properties (Shoji & Langway Jr., 1985); carbon dioxide concentrations from extracted gases (Stauffer et al., 1985); ice core dating from both δ^{18}O records and flow model analysis (Dansgaard et al. (1985) and Reeh, Johnsen, and Dahl-Jensen (1985), respectively); among others. Additionally, Dye 3 was the focus of an investigation of dust and microparticle size distribution, as well as chemical impurity concentrations, throughout climate

variations (Steffensen, 1995, 1997). Prior analysis of Dye 3 has been critical in advancing the study of paleoclimatology in Greenland and has laid the groundwork for presenting the new Continuous Flow Analysis of the 40 year old ice, on which this study is based.

1.3 Project Framing

This project is a result of the Continuous Flow Analysis (CFA) melt campaign conducted in the fall of 2019 at the Physics of Ice, Climate, and Earth section of the Niels Bohr Institute at the University of Copenhagen, in Copenhagen, Denmark. The aim of the campaign was to use high resolution CFA techniques to develop an updated and as complete as possible of a record of the Dye 3 ice core sections that have been in archive storage in both the United States and in Denmark during the nearly forty years since its drilling and retrieval from Southern Greenland. The campaign made use of CFA techniques to obtain a record of impurities and ice chemistry, atmospheric gas composition in the form of methane concentrations and nitrogen isotope analysis, as well as an investigation of improved gas extraction techniques, and water isotopes. The following report is a presentation of results from the ice impurity and chemistry data collected.

The CFA campaign included participation by multiple researchers working together on multiple different projects. The laboratory part of the campaign is the result of a considerable collaborative effort: it took place over the course of six weeks, with the participation of more than 20 scientists from more than 11 countries, melting over 500 meters of ice from two ice cores from two ice sheets in two hemispheres. For the duration of the project, there was one team dedicated to preparing the ice for melting, another team tasked with collecting water isotope data, a third team handled the gas extraction process, methane, and nitrogen data collection, and a fourth team, myself included, stationed to monitor the ice, oversee the chemistry data collection, and obtain discrete melt samples for future analysis.

The processing of the chemistry data has been a cooperative effort as well. Aylin De Campo (visiting lab intern from the University of Graz, Austria) and I worked together, with the support of our supervisors and advisors, Helle Kjær, Paul Vallelonga, and Anders Svensson, to process the veritable mountain of CFA chemistry data resulting from this campaign, in support of our respective projects. In order to support the collaborative spirit of this project, as well as to maintain a appropriate division of work for our projects, I focused on the development of a depth and age scale for the Dye 3 data and the processing of the

data, while Aylin was tasked with producing calibration curves from the standards data collected over the course of the campaign.

2. Background

2.1 Ice cores and paleoclimatology

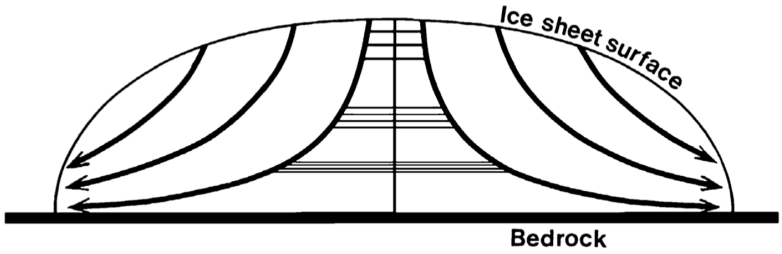

Figure 3. Idealized schematic diagram showing the layer thinning and ice flow characteristic of large ice sheets such as the Greenland Ice Sheet. Bold curved arrows show the direction of ice flow, while thin horizontal lines indicate the vertical thinning and horizontal stretching of annual layers within the ice. The vertical line in the center of the diagram indicates the location of the ice divide (Reproduced from Svensson (2014))

Paleoclimatology is concerned with the reconstruction of past climates using information stored in nature through climatic, geological, and biological processes. Some of the most important and best-preserved archives used today are ice cores. As snow falls on land in the polar regions, where conditions are favorable for snow cover to persist year-round, layer-upon-layer of snow accumulates year annually. The topmost layers weigh down those underneath, eventually generating enough pressure to squeeze the snow into ice (at 917 kg/m^3). As these layers of snow-turned-ice are compressed, the ice flows from the central divide towards the margin, each layer thinning vertically and stretching laterally as the layers above force it downwards (Figure 3) (Svensson, 2014; Bradley, 2015).

When snow falls on the surface of the ice sheets, it carries small amounts of impurities picked up from the atmosphere. Additionally, some atmospheric particles that simply settle out onto the surface of the snow. These impurities accumulate in the ice sheet stratigraphy, a record of what was in the atmosphere when the snow making up that layer of the ice fell (Steffensen, 1997; Kreutz & Koffman, 2013; Schüpbach et al., 2018). Due to this ability of polar ice sheets to store annual stratigraphic records, they are ideal sources of information about past climates. Small bubbles of atmospheric gases become trapped within the ice as the snow is compressed, preserving additional information about past atmospheric gas composition. The isotopic composition of the ice, as well, contains information

about the climate conditions at the time the snow fell (Bradley, 2015). In order to study the stratigraphy contained within the ice sheets, extensive field work is conducted to drill and remove deep cylindrical ice cores to be analyzed in a variety of ways (Dansgaard, 2004). All three of these climate records were collected in the 2019 Dye 3 ice core CFA campaign. The impurity and chemistry record will be the primary focus of this introduction, as it is relevant to the scope of this project.

2.2 Glaciochemistry and climate proxies

2.2.1 Terrestrial dust

One of the primary impurities measured in ice cores is continental mineral dust. For simplicity, the term "dust" here is used in reference to insoluble particulate matter deposited on the ice sheet surface as atmospheric fallout (dry deposition) or washed out in precipitation (wet deposition) (Steffensen, 1997). In addition to the microparticles themselves, Calcium (Ca^{2+}) is often used as an indicator of terrestrial dust aerosols, as a considerable amount of the continental dust is calcium rich mineral material (Fischer et al., 2007; Kreutz & Koffman, 2013). It is well documented (in Biscaye et al. (1997), Steffensen (1997), Mahowald et al. (1999), Ruth et al. (2003), Fischer et al. (2007), Simonsen et al. (2019), among others) that the absolute levels of dust found in Greenlandic ice cores is one to two orders of magnitude times higher in ice from the Last Glacial Period than in Holocene ice. This considerable difference in dust concentration is still not totally understood, but has been hypothesized to be due to a higher level of storminess and aridity causing more dust to be swept into the atmosphere from continental sources (those sources themselves larger during glacial climates due to lowered sea level and exposure of continental shelf), dryer climates leading to less precipitation induced washout during transport towards the polar region, and changes in atmospheric circulation patterns and intensity (Biscaye et al., 1997; Steffensen, 1997; Ruth et al., 2003).

Studies have examined changes in dustiness and identification of dust sources using atmospheric modeling and analysis of the mineral and isotopic composition. They have found that while the dust concentration is higher during glacial periods, it is likely that the source has remained the same, and that changes in continental climate conditions and atmospheric circulation intensity are likely to be the most significant contributors to the difference in dust concentrations (Biscaye et al., 1997; Steffensen, 1997; Mahowald et al., 1999; Fischer et al., 2007; Schüpbach et al., 2018). It is due to these findings, that dust

and calcium in ice cores are often used as proxies for windiness, continental aridity, and atmospheric circulation intensity.

Due to the glacial expanse of the Greenland Ice Sheet, there are no dust sources local to its interior. Therefore, the terrestrial dust found in the Greenlandic ice must have come from somewhere else. The provenance of this ice core dust has been the subject of prior analyses. Possible source areas for the dust found in Greenlandic ice cores have been studied by matching the mineral and isotopic characteristics of the ice core to samples taken from continental deserts and other source areas (Biscaye et al., 1997; Simonsen et al., 2019). Despite the existence of many more proximal deserts dust source areas, dust from Greenlandic ice has been sourced to Eastern Asia, particularly the Chinese Loess Plateau and Gobi Desert. Additionally, atmospheric modeling has been used to determine the that enable transport of dust to Greenland from these faraway regions (Biscaye et al., 1997; Mahowald et al., 1999).

2.2.2 Sea salt

In addition to insoluble particles, ionic species are also used as proxies in ice core climatology. One such proxy often studied is sea salt. Sea salt aerosols are most commonly measured with CFA using Sodium (Na^+), as well as Cl^-, K^+, and Mg^{2+} (the latter often measured using ion chromatography) (Legrand & Mayewski, 1997). It would make sense that sea salt aerosols would be dominant during warmer times with less sea ice due to the aerosolization of seawater in wave action in open water. However, it is conversely found that levels of sodium are typically higher during colder Glacial (and Glacial Stadial) climate periods, in addition to being observed in winter peaks (Kreutz & Koffman, 2013). This is thought to be due to a combination of increased storminess during colder periods causing more seawater aerosolization, but also due to the release of sea salt aerosols from "frost flowers" formed in the sea ice crystallization process and the strong salty brine produced in the formation of sea ice (Fischer et al., 2007; Kreutz & Koffman, 2013; Schüpbach et al., 2018).

2.2.3 Forest fires and biogenic signals

Another event response seen in Greenland ice cores, but on a much shorter time scale, is the signal of large-scale forest fires, specifically boreal forest fires and other large scale burning of biomass at high northern latitudes. Using CFA techniques, the biomass burning signal of forest fires is mostly measured using Ammonium

(NH_4^+), which sharply increase during fire events. In addition to these spikes, there is also a background signal of NH_4^+ due to biological emissions, largely soil respiration, decomposition, and vegetation (Legrand & Mayewski, 1997; Kreutz & Koffman, 2013; Schüpbach et al., 2018; Fischer et al., 2015; Legrand et al., 2016). It therefore follows that during glacial conditions, there are seen to be lower concentrations of ammonium in Greenlandic ice than is seen in Holocene and Eemian (warm period) ice. This is attributed to the widespread ice sheet cover during glacial periods, particularly the Laurentide Ice Sheet, suppressing soil respiration and eliminating large swaths of the northern hemisphere that would otherwise support vegetation (Kreutz & Koffman, 2013; Fischer et al., 2015; Schüpbach et al., 2018).

2.2.4 Volcanic signals

Large volcanic eruptions, which are also short term signals, can be seen in ice core records as well. When volcanoes erupt, they emit substantial amounts of aerosols, in the form of both gases and particulate matter, injecting these aerosols into the atmosphere at various levels (Kreutz & Koffman, 2013). The signatures of these volcanic eruptions is typically studied with CFA analysis using sulfate concentrations and ice acidity (mostly using sulfuric acid). Volcanic eruption layers, however, can also be pinpointed through the identification of particulates including volcanic ash and tephra, volcanic glass shard particulates spewed into the air during eruptions (Kreutz & Koffman, 2013; Bourne et al., 2014). In Greenlandic ice cores, largely due to the proximity to Iceland, many volcanoes are seen with both regional as well as global impact, while due to the continent's isolation, Antarctic ice cores typically only show global scale eruptions (Kreutz & Koffman, 2013). Volcanic fingerprints in the ice are incredibly useful in synchronizing the dating of ice cores from various locations. While localized eruptions can be useful in linking the stratigraphic record of the different ice core sites in Greenland, the large global scale eruptions can be used in synchronizing the chronologies of Greenland with Antarctic ice cores (Vinther et al., 2006; Bourne et al., 2014; Rasmussen et al., 2014; Svensson, 2014).

2.3 Continuous Flow Analysis (CFA)

Continuous flow analysis is a method of analyzing ice cores with very high resolution, while reducing time and effort involved in sample decontamination. In the CFA process, pioneered by Sigg et al. (1994), a section of an ice core, cut

lengthwise along its axis, is placed on a warmed plate (the melt head), and melted from one end to the other (typically from the top down). The meltwater is then collected and simultaneously analyzed as it is pumped through a system of measurement instruments. The speed of melting can be controlled by the temperature of the melt head, and the external portion of the core section can be diverted to prevent contamination from entering the sample stream. The meltwater is transported by peristaltic pumps and diverted via valves and manifolds through lengths of tubing to instruments which continuously and simultaneously measure different characteristics (impurities, isotopes, etc.) at regular time intervals (typically each second). For measurements that require it, separate reagent and buffer compounds for each measured impurity are continuously pumped into the system in line with their respective measurement streams, with appropriate mixing coils, etc., prior to fluorescence or absorption measurement instruments (see methods section for a more detailed description of the CFA setup used in this campaign). Through CFA, the data can be collected remarkably efficiently and can be reconstructed onto a depth scale of very high resolution - down to the millimeter scale - for entire lengths of deep ice cores. As CFA requires melting of the ice sample, and is therefore a destructive technique, the melt stream can be segmented with a portion diverted towards collection vials to retain samples for further analysis or archival purposes.

The CFA system setup is quite modular, and while it can be simple and efficient enough for deployment to the field for in-situ measurements, it also can be expanded to measure numerous parameters simultaneously and is well suited for use in a lab environment. CFA systems can also include the use of gas extraction systems and cavity ring down spectrometers to continuously measure gas composition and gas or water isotopes, respectively. In addition, autosamplers can be used to collect frequent discrete samples for ion chromatography or ICP-MS measurements to be performed later. When compared with the traditional discrete measurement procedures, CFA requires significantly less handling of the sample ice, allowing for more measurements, thus higher resolution, as well as more efficient sample decontamination.

The CFA setup used in the 2019 Copenhagen campaign (Figure 4) has been modeled after a similar system at the University of Bern, Switzerland, and modified following many of the descriptions of Röthlisberger et al. (2000), Kaufmann et al. (2008), Bigler et al. (2011).

3. Methods

Ice was melted at the section for the Physics of Ice, Climate, and Earth (PICE) at the Niels Bohr Institute the University of Copenhagen using a CFA system, during October and November of 2019. Throughout the course of the campaign, over 100 sections of ice were melted, each originally approximately one meter long, covering roughly 67 meters of ice from the Early Holocene and Glacial Transition (1753.5-1820.4 meters depth) and 53 meters of ice from the Glacial (1865.3-1918.3 meters depth). The melting was completed over the course of 15 "runs" of continuously melted ice over the course of two weeks.

3.1 Laboratory Procedures

3.1.1 Ice Preparation

The ice from the Dye 3 ice core was cut in the field into sections of approximately 1 meter long (the standard used by American ice core scientists), referred to here as "bags" based on their storage method. Prior to CFA melting, the ice must be prepared in a cold room kept at approximately -20°C. Longitudinal sticks of ice are cut with cross-sectional dimensions of 35mm x 35mm. While each "bag" was approximately 1 meter long in the field, due to the long storage time and transportation from freezer to freezer over the last 40 years, the majority of the bags had multiple breaks within each bag. Additionally, there are doubtless some sections with breaks that had been re-frozen or subjected to sublimation or accretion of ice during the long storage time.

At the top and bottom of each bag, as well as at each break in the ice, a thin layer of ice must be removed in order to eliminate possible traces of contamination and to ensure proper alignment of the pieces within the frame. This cleaning of the ice is done by carefully shaving off fine layers of ice using a microtome knife. The length of ice and position of each break are carefully noted prior to any cutting, and a careful record of the amount of ice removed at each break is kept, as well as measurements of the position and length of each break after cutting and cleaning the ice. [See appendix for an example of log sheets used to record the ice preparation for each bag.]

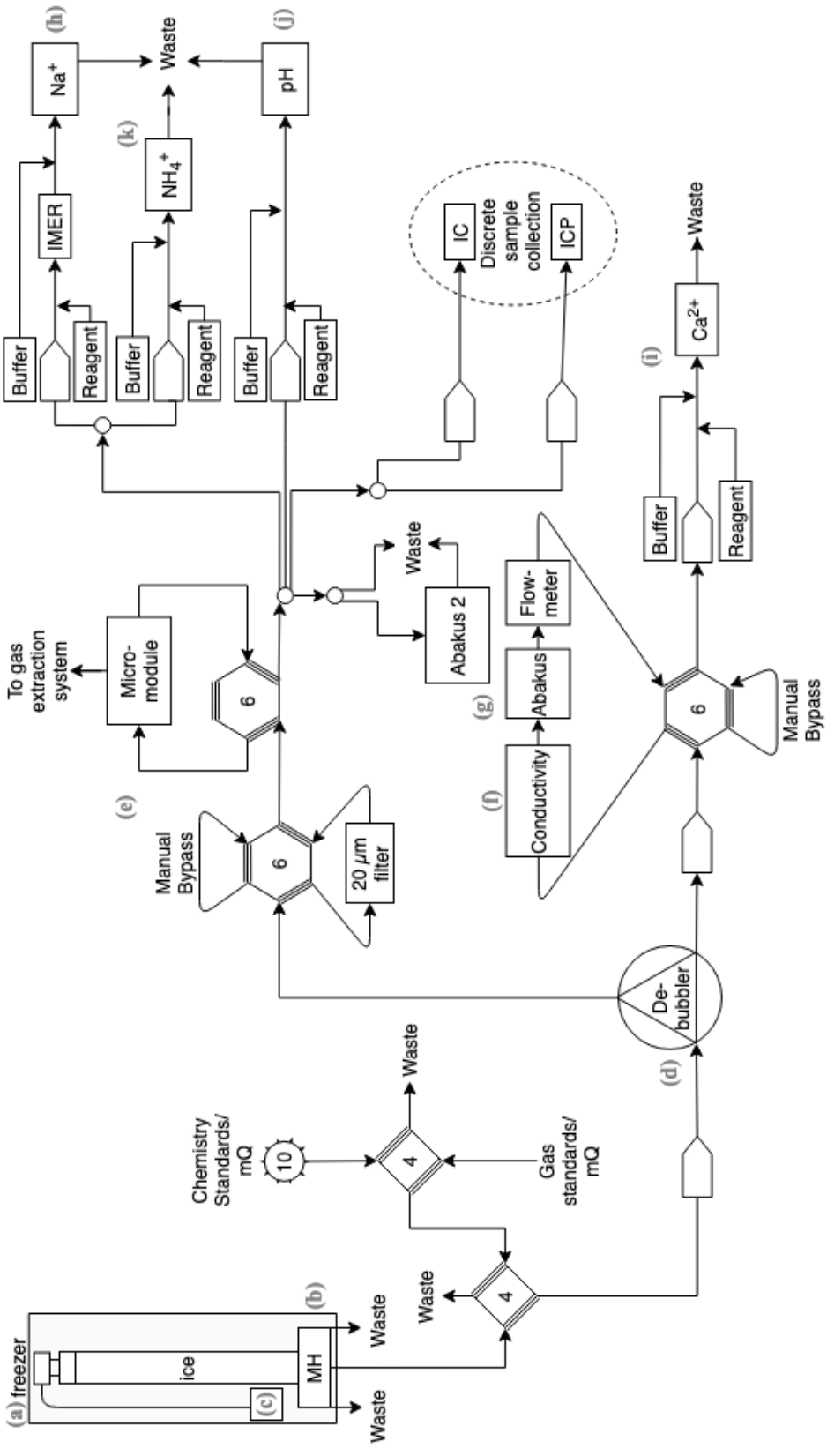

Figure 4. Simplified diagram of the setup used in the 2019 Copenhagen CFA campaign. **a.**) Freezer, **b.**) Melter, **c.**) Encoder system, **d.**) Debubbler, **e.**) Gas extraction system, **f.**) Conductivity meter, **g.**) Abakus laser particle meter, **h-k.**) Chemistry measurement instruments.

3.1.2 System control and data collection

The CFA system, including manifold valves, is controlled and operated on a PC using LabView software. In this way, the valves are controlled for both the sample melting and the standard runs. LabView is used to collect and record the data as well as the start of sample melting, breaks in the ice, and the beginning of each new bag. Notes are also recorded in a laboratory notebook. Finally, bag mean samples are collected in vials to act as an archive and for potential future measurements.

3.1.3 System setup

Freezer. The ice is placed in transparent polycarbonate frames, mounted vertically within a freezer kept at approximately -20C (Figure 4a). The freezer is a commercial beverage cooler that has been outfitted with a support structure for the ice frames, as well as an insulated box containing the heating elements of the melter and outlet for the tubing that collects and transports the meltwater to the CFA system. The glass door of the freezer allows the melt progress to be carefully monitored throughout the duration of the melting, in addition to allowing easy access for correcting ice alignment and changing frames.

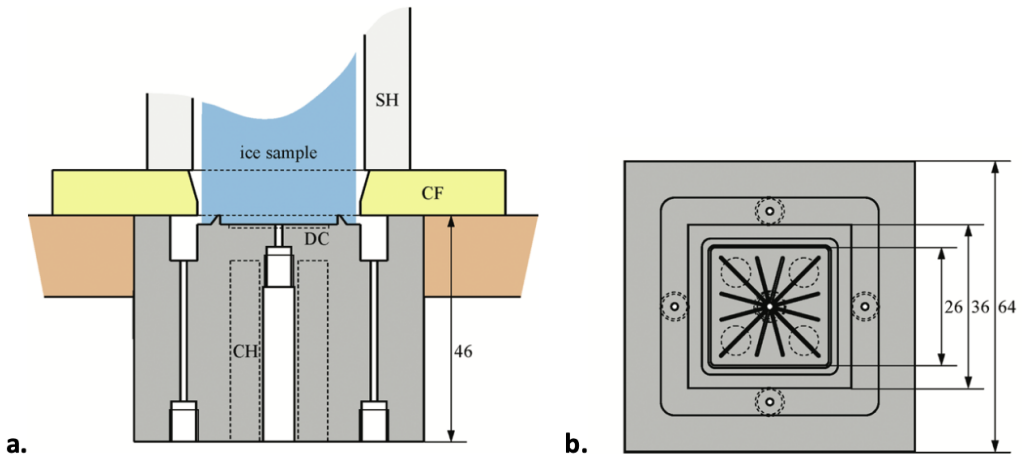

Figure 5. a. Schematic diagram of a melter unit similar to the one used in the Copenhagen CFA system. **b.** Melt head diagram with dimensions shown. DC = drain channel; CH = cartridge heaters; CF = centering frame (not used in 2019 Copenhagen CFA setup); SH = sample holder; measures are in mm (reproduced from Bigler et al. (2011)).

Melter. When melting begins, the ice is lowered on to a melt head (Figure 4b, detail Figure 5), which is heated to a designated temperature, typically

between 40-50℃for this campaign, to maintain desired melt speed. Pressure on the melt head is maintained by the weight of the ice as well as an added weight to which the melt-speed encoder system (described below) is attached. The melt-head is designed specifically to separate the meltwater flows from the exterior and interior of the ice to prevent possible contamination from the exterior of the CFA stick.

The exterior melt flow is passed to waste or to other contamination insensitive measurements (e.g. water isotopes). The interior flow is passed to the CFA system for measurement. The meltwater is transported through the system using a series of peristaltic pumps, the first of which is calibrated to pull a lower volume from the interior than is produced by melting, thus causing a consistent small amount of overflow from the inner section to the outer section, further preventing contamination from the outer section.

Melt speed and Encoder. In order to record the speed of melting (determined largely by the melt-head temperature), and thus the length of ice melted, an encoder is used (Figure 4c). This melt speed is used in the creation of a depth scale. The encoder consists of a cable attached to a weight that is placed atop the ice in the freezer and an optical sensor, which records the encoder position based on the length of the cable from the sensor to the attachment point on the weight, as well as the position differential. The encoder measures the melt speed in 'clicks' per second. When the frame is changed, the encoder cable must be removed, and subsequently replaced once new ice is added to the freezer, thus disrupting the encoder measurement. This proves problematic for creating a continuous measurement and is described in more detail later.

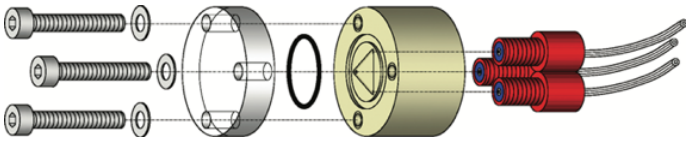

Figure 6. Diagram of a sealed debubbler unit, similar to the one used in the Copenhagen CFA system (reproduced from Bigler et al. (2011)).

Debubbler. As the ice melts, tiny pockets of trapped air (past atmosphere) are released. For chemistry measurements, these air bubbles must be removed to prevent bubbles in the measurement lines. Since the Dye 3 melt campaign was a combined chemistry and gas measurement campaign, the gasses were extracted and removed for analysis simultaneously to the chemistry analysis. One way to remove air bubbles from the ice is a debubbler (Figure 4, detail Figure 6). A simple device, the debubbler consists of a sealed flat triangular cell with one

inlet and two outlets, each at one corner of the triangular cell. The triangular cell is oriented with one outlet at the topmost corner of the triangle, and the inlet and remaining outlet at the bottom two corners, respectively. This orientation, together with calibrated pump suction pressure allows bubbles to rise to the top of the cell and, together with some meltwater, to be removed by the outlet at the peak of the triangle, while the lower outlet then transports the remaining bubble-free melt flow.

For this campaign, the introduction of a gas-extraction micro-module was used in addition to the debubbler. The debubbled melt stream (in this case only a small fraction of the total melt) is passed on for measurement of insoluble particles, conductivity, and Ca^{2+} (described below), while the remaining meltwater and air, from the top outlet of the debubbler, are passed through the gas extraction unit (Figure 4e). Once the gasses are removed, it continues to the remaining chemistry setup. As this project is not specifically concerned with the gas measurements of Dye 3, the micro-module and gas extraction system will not be discussed here. The setup is described in more detail in the recent M.Sc. thesis of Janani Venkatesh (2020) (see appendix for gas extraction setup diagram).

Dust measurement. The insoluble particles are measured using an Abakus laser particle sensor (Klotz GmbH, Germany, Figure 4g). The Abakus measures the number of particles passing through the laser beam per second, and as such, a flowmeter is set in line just past the Abakus, in order to later convert particles per second into particles per milliliter, then per millimeter of ice melted. Additionally, the Abakus measures the size distribution of the particles as they pass through the laser beam. In order to determine the impact of the gas extraction micro-module setup on the microparticle measurements, two Abakus instruments were used in this setup, one recieving flow from the debubbled sample stream after the debubbler, and a second instrument after the gas extraction system. A 20 micron filter was included prior to the gas extraction system, and despite the fact that the largest particle diameter measured here is 15 microns, it was determined that in order to minimize possible interference in the signal, the Abakus on the debubbled sample stream would provide a truer measurement of the microparticle concentration. Therefore, all Abakus data used in this report is from this instrument.

Meltwater electrolytic conductivity. Electrolytic conductivity is a good representation of the bulk signal of the ionic components contained in the ice. A simple conductivity cell is used in this setup (Figure 4f), and conductivity is measured in units of µS/second. The conductivity meter is on the same line, just

prior to the Abakus instrument.

Chemistry measurements. The remaining chemistry measurements are performed using either absorption or fluorescence methods of detection (Figure 4h-k).

Absorption is used to measure the concentration of sodium as well as the pH of the meltwater. The absorption method measures the amount of light absorbed by a sample as it passes through the beam of an LED with known wavelength and intensity in front of a sensor that measures the amount of light absorbed by the sample. The Na^+ measurement (Figure 4h) is an absorption technique based on an enzymatically controlled reaction with the present sodium, and thus requires the use of an immobilized enzyme reactor (IMER) column (as described in Röthlisberger et al. (2000)). The pH measurement (Figure 4i) is not a true absorption measurement, but a measurement of the color change of the sample due to the addition of a reagent with a pH indicator solution (see Kjær et al. (2016) for further information about the development of the pH detection method for CFA used here). Due to delays encountered by Aylin DeCampo during calibration, the Na^+ record is unfortunately not able to be presented here.

Fluorescence is used to measure the concentration of Ca^{2+} and NH_4^+ ions (Figure 4j&k). In fluorescence detection, molecules in a sample are excited using a LED of specific wavelength, and as they return to ground state, measurements of the fluorescence emitted by the sample are taken.

3.1.4 Run procedure

Typically, 16 bags were melted each day, in two runs of eight bags each. Each run is identified by the record number of the first bag of that run. Preceding each run, as well as at the end of the day, a standard run was performed (procedure detailed below). Melt speed was maintained at approximately 4.5 centimeters per minute, controlled by adjustments to the melt head temperature when necessary. Upon reaching the end of each bag, the support frame was replaced, containing a new piece of ice in order for continuous melting to continue. Frame changes were performed with the following procedure: When approximately 15 centimeters of ice remained in the frame, a new frame containing the next bag was retrieved from the prep freezer. The encoder cable and weight were removed from the top of the ice, and the now empty frame was removed and replaced with the new frame of ice. The weight was returned to the top of the ice in the new frame, and the encoder cable was attached to the weight. The pin holding the ice in the new frame was removed and the new ice was lowered to rest on top of the remaining section of ice

on the melt head, in order for continuous melting to continue uninterrupted. A 7 centimeter long section (or occasionally two cubes, each 3.5 centimeters long) of milli-Q ice was included at the beginning and end of each run, in order to prep the lines in the system, ensure no air bubbles remained in the system before sample melting began, and establish baseline values for some measurement instruments.

3.1.5 Standards

In order to later calibrate all data measured, standard solutions with a known predetermined composition were made and measured in the system.

Table 1. Recipes used in standard solutions. Standards concentrations used are shown in bold.

	Standard Stock (μl)	Milli-Q water (ml)	Concentration
Multielement			
Stock solution (ppb)	-	-	1000000
1st dilution	50	200	**24.6**
1st dilution	100	200	**49.2**
1st dilution	400	200	**197**
HCl (pH standard)			
Stock solution (µmol/L)	-	-	100100
1st dilution	900	30	3003
2nd dilution	800	120	**20**
2nd dilution	400	120	**10**
Na0H (pH standard)			
Stock solution (µmol/L)	-	-	100100
1st dilution	900	30	3003
2nd dilution	800	120	**20**
2nd dilution	400	120	**10**

Standard solutions are mixed prior to each standard run according to the recipes given in table 1. A multi-element standard is used to measure Ca^{2+}, Na^{+}, and NH_4^+ as well as electrolytic conductivity. This multi-element standard is prepared as a dilution in milli-Q water. Three strengths of multi-element standard are used to ensure proper calibration. To calibrate the pH measurements, two different sets of standard solution are used to provide pH measurements in terms of µM H^+. Two strengths of HCl are used to calibrate for acidity and two strengths of NaOH are used to calibrate for alkalinity. All four pH standards are prepared as second dilutions, of HCl and NaOH, respectively. The first dilution of each is prepared daily, while the second dilution is prepared immediately prior to

each standard run.

Standards runs are typically performed three times per day: once before the beginning of melting at the beginning of the day, once upon completion at the end of the day, and once in between the two runs of the day. All standard solutions share one valve, controlled remotely by the LabView software. Each standard is run in series, beginning with the three strengths of multi-element standard, followed by the two acidity and two alkalinity standards. Each standard is measured for 180 seconds, and values are recorded on a log sheet as a backup to the computer recorded data.

3.2 Data processing

Data processing was completed in MATLAB. Scripts were written specifically for this analysis, based on methodology used in previous CFA melt campaigns.

3.2.1 Depth Scale

In order to analyze CFA data, the collected encoder measurements must be used to convert the data from an acquisition time scale to a length scale (representing the length of ice melted in the laboratory), then to a depth scale (representing the depth within the ice core to which each measurement corresponds). In order to create this depth scale, the encoder data that was collected as an encoder position and a melt speed in "clicks per second," must be converted into a length. For periods of measurement during which the ice melted and the encoder was able to collect data uninterrupted, this simply involves using a conversion factor (specific to the encoder instrument used) to convert from "clicks per second" to millimeters per second, then using the acquisition time to convert to length of ice measured.

Frame changes. Trouble arises when the end of a bag is nearing and the frame must be changed. During a frame change, the encoder is removed from the top of the ice in order to replace the now empty frame with a new one containing the next ice to be melted. This exchange takes place just before the end of the current bag is reached, ensuring continuous melting from one bag to the next. While the frame is being changed, the ice remaining on the melter continues to melt, despite the fact that the encoder is not registering any movement.

This missing data must be accounted for in processing in order to create a smooth, continuous depth scale, and is done here using the following methodology: The encoder height data is used to determine a threshold value which is only crossed by the encoder during the frame changes (once as the

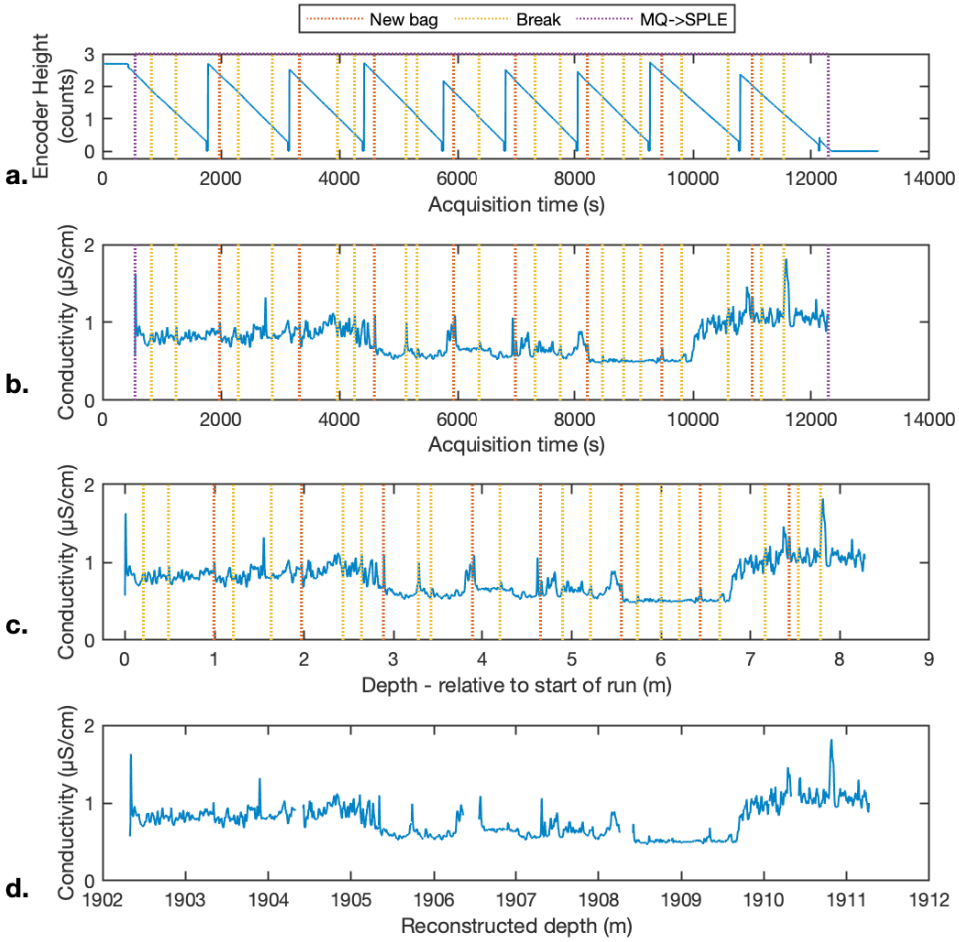

Figure 7. Demonstration of the depth scale creation process. **a.** Encoder height raw data plotted on acquisition time scale. Shown here with sample start and end (when the "Milli-Q to Sample" button was pressed), as well as each new bag and break record. **b.** Raw conductivity data plotted on acquisition time scale with new bag and break records. **c.** Conductivity data plotted against relative depth scale. The start of the bag is set to zero and the encoder data is used to convert melt rate to depth after interpolations have been made to account for frame changes at each new bag. New bag and break records shown. **d.** Conductivity data plotted against final depth scale for the run. Breaks have been added according with methods procedure, and the start of each new bag has been set to the bag top depth corresponding with that bag. Note the gaps in the data where ice was removed at breaks.

encoder is lowered to its lowest position as it is removed and again as it is raised to be replaced at the top of the new frame of ice during the frame change). The points at which the encoder crosses this threshold are considered to be the start and end of each frame change, and a buffer of 30 seconds is added before and after this period to account for any delays or shifting of ice related to the frame change

procedure. With the assumption that the melt rate remains constant during the frame change, the encoder-recorded melt rate is then interpolated across the period of time designated as the frame change. The addition of the milli-Q ice cube at the end of each run also poses a challenge for generating consistent encoder data. During some runs, the encoder is removed completely when the milli-Q ice is added, allowing it to be treated as a typical frame change. Other times, however, the encoder is not lowered to its lowest point during the milli-Q ice addition, and therefore the start and end of the time period must be chosen manually. After all frame changes and the milli-Q addition are accounted for, the melt rate data may be converted to a length of ice melted, as described above.

Encoder problems. There were four runs during the course of the Dye-3 melt campaign during which the encoder encountered problems or stopped working completely. Coincidentally, in each of these cases, the encoder problems occurred during the third bag of the run. During three of the problematic runs (run numbers 1825, 1828, and 1831), the encoder stopped responding and failed to continue recording the encoder height or melt rate, while in the fourth problematic run (1862), the cable on the encoder hardware snapped, causing the encoder to register false data for the remainder of that run. In all three cases, the run was terminated upon the completion of the current bag (including addition of a milli-Q ice cube), and troubleshooting and repairs or replacements were conducted prior to beginning the next run. During data processing for these problematic runs, the melt rate for the period after the problems occurred was considered to be the average melt rate for the length of the bag preceding the loss of encoder data.

Break reconstruction. In addition to frame changes, the conversion from the length of ice melted in the laboratory to a depth scale must account for breaks in the ice and any ice that is removed in an attempt to rid the breaks of possible contamination and ensure alignment of ice pieces within the frame. During the preparation of the ice, careful measurements are taken both before and after any cutting takes place in order to maintain an accurate record of the position and length of any segments of the ice that are missing or removed. These logs are then used in the creation of the depth scale, adjusting the depth to include the missing ice. The missing ice is added from the bottom to the top for each run, by identifying each location a break is recorded, and adjusting all depths after that point by the amount that was recorded as removed. In this way, gaps are introduced into the data at the appropriate places.

Depth assignment. Due to discrepancies between logs containing measurements taken at different times during the course of the Dye 3 core's 40

years in storage, considerations had to be made in assigning depth to positions in the recorded ice length. As small errors in measurement could compound over the length of the measured ice, it was determined that the depth recorded in the field at the time of drilling for the top of each bag recovered should be used to prevent this compounding error. Therefore, in determining the depth scale, the top of each bag was assigned to the bag top depth recorded for that bag. While this could potentially lead to unused data or gaps in the CFA record, it was decided as the best way to create a depth scale that could be used to facilitate the truest comparison of this CFA record with previously measured data from the Dye-3 core.

3.2.2 Age scale

As the official age scale for Dye 3 only covers the Holocene, a preliminary age scale was created for this data by Anders Svensson and Bo Vinther. This age scale combines volcanic events and D-O event transitions for a set of match points with the NGRIP ice core extending through the measured length of Dye 3 as presented here (see Appendix for match points used). In order to use the most complete age scale, the official GICC05 age scale for Dye 3 (Rasmussen et al., 2007) was used for the extent that it covers, and the rest of the record used the preliminary age scale as described.

3.2.3 Delay times

Due to variation in the length of tubing, mixing coils, and heating/cooling elements connecting the measurement instruments, there is a delay in response time between the different species measured using the CFA system. Since the data is acquired at regular time intervals (1 second), it is imperative to understand and quantify this delay time in order to synchronize the records for each component. This delay time is calculated as follows. First, the data from each standard run is used. Since one of the standards used is a multi-component/multi-element standard, it is possible to determine the difference in response time between each responding element and the conductivity response time, as conductivity is the closest to the melter and thus the first measurement to respond. For measurements that do not respond to the multi-element standard (acidity and alkalinity), the programmed time delay between the onset of the multi-element standard and the desired standard can be used.

Second, the delay time of the conductivity measurement, however, must also be calculated. The elapsed time between the start of the sample melting and

the observed response in conductivity as the sample reaches the conductivity meter is considered to be the conductivity delay time for that run. As the Abakus and the conductivity meter are sufficiently close together, and display similar response time, the difference in delay times is seen to be negligible, and the same delay time is used for both conductivity and dust (see Appendix for all delay times used).

3.2.4 Baseline drift

As some impurities have a tendency to settle out and accumulate in the tubing used in the CFA system, it is common to see a drift in the baseline value recorded over the course of a run for some species. In order to remove this drift, a baseline value is computed from the period of "blank" mili-Q water run through the system before and after each run. The "before" baseline value is typically computed from the baseline immediately prior to each run. Since the measurement can take a few minutes to reach equilibrium, the "after" baseline value is computed from the baseline data only once the baseline has appeared to level off. In the case of runs where the data collection was cut off before "true" baseline was reached, the baseline was computed from the next file saved immediately following the run (either the subsequent run file or the following standard file). The slope of the baseline is then computed and subtracted from the data throughout the duration of the run. Calcium and pH most frequently result in signal drift that must be corrected for. The drift in the pH signal is typically most pronounced during the standard runs.

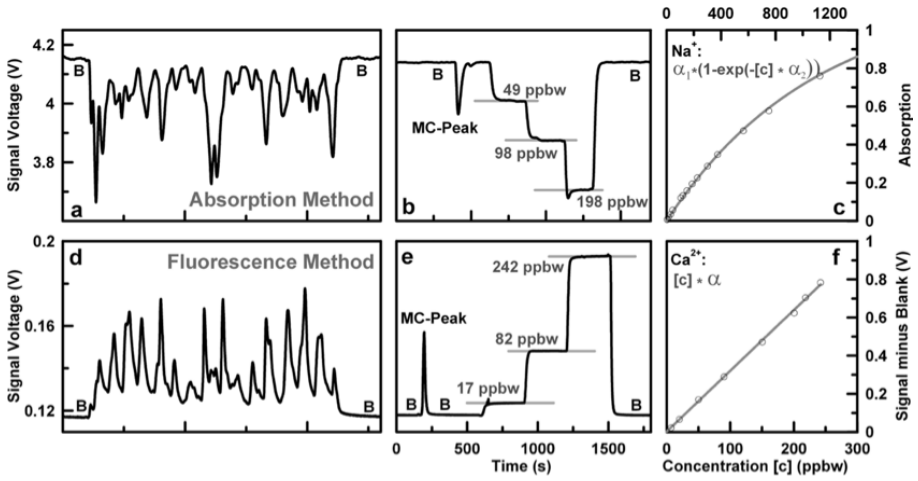

Figure 8. Characteristic example of data from absorption (**a**) and fluorescence (**d**) detection methods, as well as corresponding examples of standard runs for each method respectively (**b** & **e**) and calibration curves produced from the standards data (**c** & **f**). In plots **a**, **b**, **d**, & **e**, baseline values are marked with a "B".

3.2.5 Standards and data calibration

The species measured using absorption and fluorescence methods produce data in units of photon counts per second, and therefore must be converted into concentrations in order to produce meaningful results. In order to perform this conversion, the instruments must be calibrated with standard solutions with known concentrations of each species (Table 1) using data from the previously described standard runs. As the standards concentrations are known, it is possible to use this standard run data to calculate a calibration coefficient as well as a baseline response value for the Milli-Q water.

In the calibration process, standard run data is used to establish a corresponding concentration value with the resulting signal response. This data can be plotted, and a calibration curve can be fitted to determine the relationship as follows.

Fluorescence method. As the fluorescence method, used for Ca^{2+} and NH_4^+, results in a linear calibration curve, the following equation is used in the calibration process:

$$I - I_0 = \epsilon * c * l$$

In which the baseline, I_0, must be removed from the signal, I, to equal the product of the concentration, c, the molar extinction coefficient, ϵ, and the length of the measurement cell, l. In order to create a calibration curve, the standard response signal values are plotted against their corresponding concentrations, and a curve is fit, as in Figure 8 in which the slope is equivalent to the calibration coefficient, alpha, which is equal to $\epsilon * l$. Therefore, the following equation is used to generate calibrated data:

$$F = (I - I_0)/\alpha \tag{1}$$

Absorption method. Sample pH is measured based on a color change resulting from the reaction of the sample to a reagent containing an indicator dye, which is passed through an absorption cell. Therefore, although not a true absorption method, the data is treated in much the same way as a typical absorption method. Unlike the fluorescence method, the absorption calibration data follow a log-linear relationship, therefore the baseline must be removed using a logarithmic method. The data signal, however, falls in the linear range of the calibration curve (seen in the lower portion of Figure 8), and therefore can be assumed to be linear, resulting in the following equation for the data calibration:

$$F = log(I/I_0)/\alpha \tag{2}$$

The standards calibration calculations were performed using a MATLAB script written for this purpose. As this was a collaborative project, the standards calibrations were performed by Aylin De Campo, as a part of her thesis work, and thus will not be discussed in further detail here. Standard calibrations (as provided by De Campo) can be seen in the Appendix.

3.2.6 Ammonium corrections

Due to the particulars of the ammonium setup, the ammonium data is expecially succeptible to air bubbles passing through or getting stuck in the sensor, causing false spikes in the data. In most cases, these spikes are easily identified as single data point jumps to values well above the signal range. These erroneous spikes were simply identified by taking the differential of the ammonium signal, and removing points that correspond with differential values above a certain threshold (well above that seen in the real data signal). While straightforward, it is possible, however, that this method did not manage to perfectly account for every single unnatural spike in the ammonium data.

3.2.7 Possible contamination

There are many instances during which, typically at the locations where breaks in the ice occur, there is a spike in the impurity records that is likely due to contamination of the ice core by drill liquid, particulates introduced to the ice during handling, or another source. It is most likely that these spikes correspond with recorded breaks in the ice, despite best efforts to clean the ice during preparation. In these cases, it can be noted that the signal is likely due to contamination and the data can either be ignored or removed from the record. It is also possible, especially due to the long storage time of this particular core, that some contamination spikes may occur where there is no recorded break. This is due to refrozen breaks that were not caught during ice preparation or thin ice sections causing misalignment on the melt head. In these cases, it is much more difficult to definitively attribute these spikes to contamination, and it is possible that such spikes go unnoticed as contamination.

In this analysis, in order to avoid discarding data that could later prove useful, or may possibly be mis-identified as contamination, no data has been removed from the record, even when impurity records spike near breaks in the ice. Therefore, care has, and must continue to be, taken in analysis to check any data spike analyzed for its proximity to breaks in the ice to avoid attributing meaning

to data that is actually a sign of contamination.

In order to have a record of possible contamination, the data was investigated to identify possible contamination spikes. The overall dust signal, as well as the signal of particularly large particles (from the Abakus binned data), were visually examined together with all recorded breaks in the ice, and any substantial spike in the data that coincided closely with a recorded break in the ice were flagged as possible contamination. As this was a simple visual inspection, it is important to note that the resulting data flagging is somewhat subjective, as it can be difficult to distinguish real signal fluctuations from significant spikes due to contamination. Additionally, not every break was recorded in the lab, so it is possible that some contamination spikes were not flagged due to lack of a complete break record.

4. Results

Results from the Autumn 2019 Dye 3 CFA campaign are presented. First, a simple representation of the depth and age scales, followed by the chemistry data.

4.1 Depth scale and depth age relationship

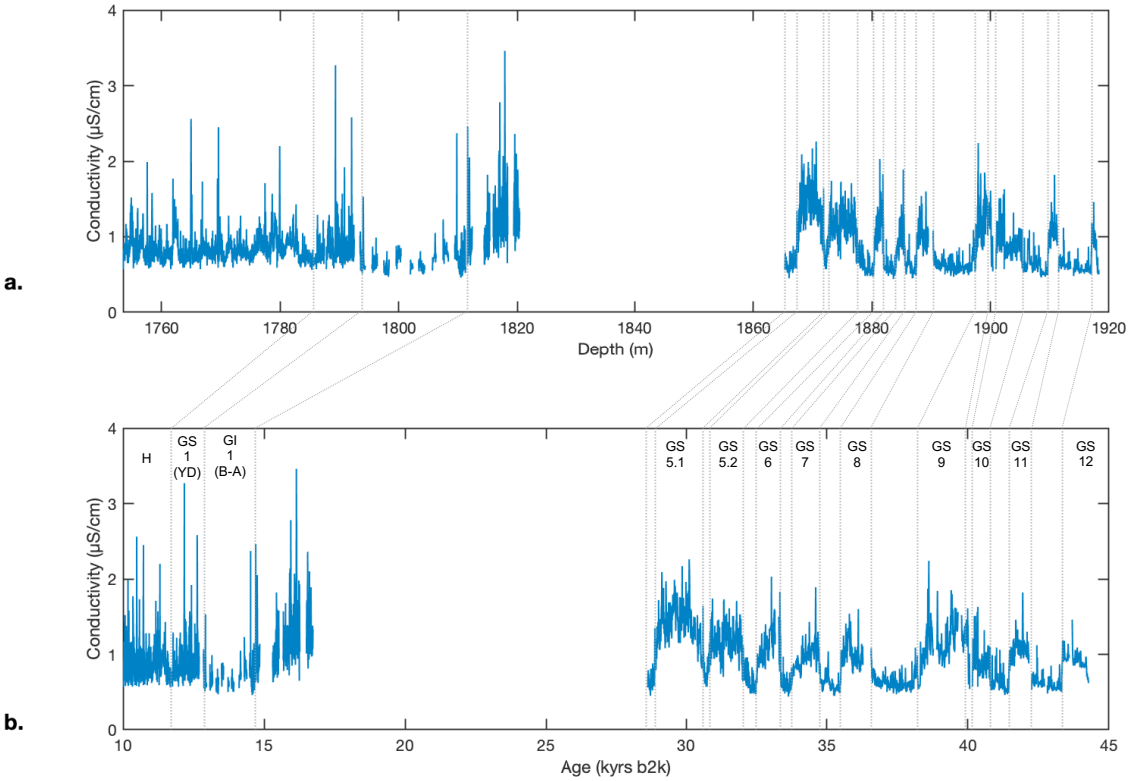

Figure 9. Age-depth relationship: Dye 3 conductivity record shown on (**a**) the reconstructed depth scale and (**b**) the age scale compiled for this project (combined from Rasmussen et al. (2007) and match points drafted by Anders Svensson and Bo Vinther (personal correspondence, 2020)). Greenland Stadial (GS) and Greenland Interstadial (GI) onsets are marked according with their ages and names in accordance with Rasmussen et al. (2014).

The comparison of the depth scale and the age scale (Figure 9) appears as expected, with the Glacial-Holocene transition and D-O events appearing at the expected time periods. Gaps exist in the data where sections of ice core were missing, damaged, or too small to be used. However, as seen on the depth scale, there exists a section of data covering the early Holocene (H) and Glacial Transition (Younger Dryas (YD) and Bølling-Allerød (B-A)), as well as a section of the Last Glacial Period covering Greenland Stadial periods 5 through 12.

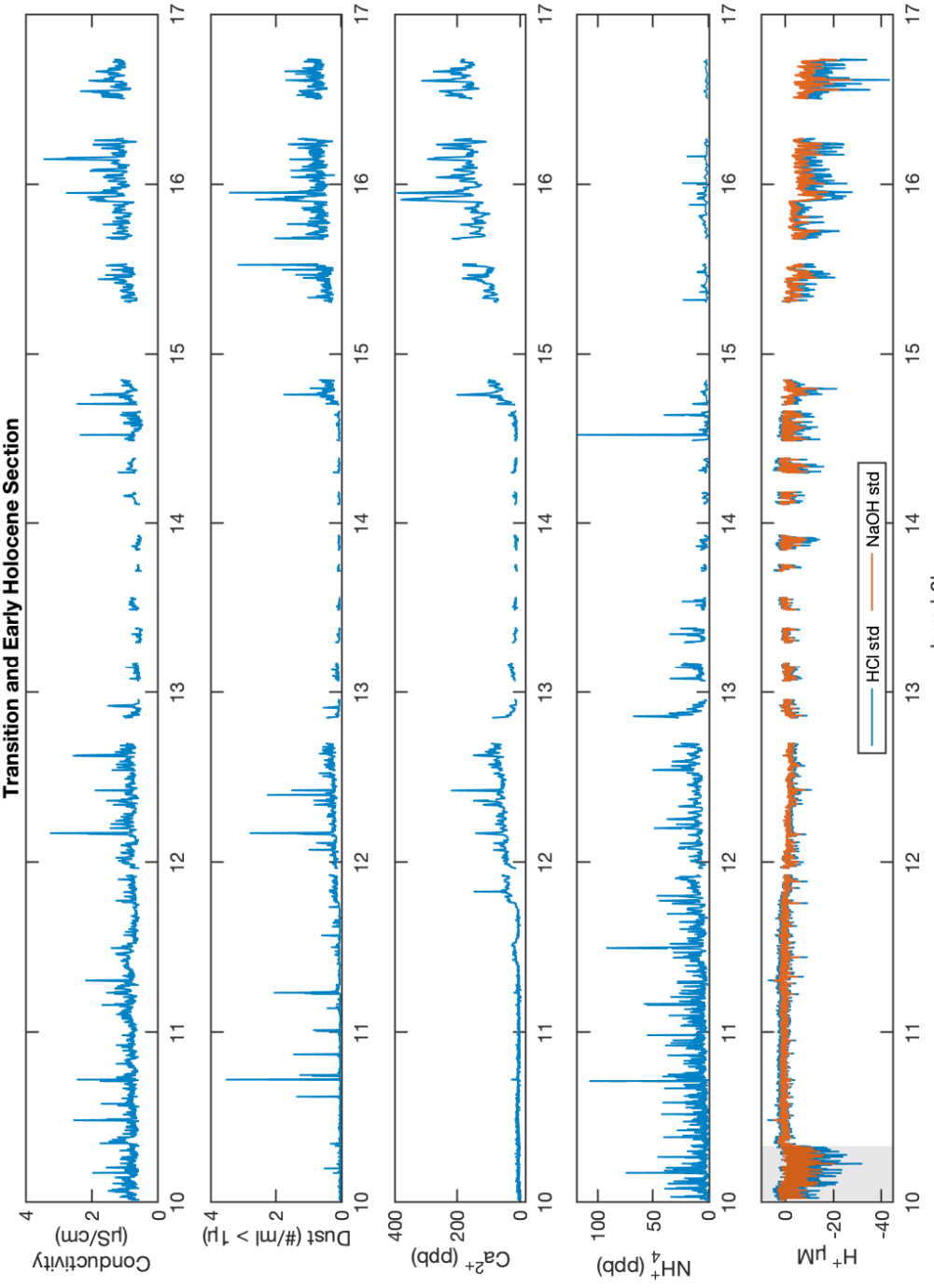

Figure 10. CFA Chemistry record for the Holocene and Transition section of Dye 3, shown here on a modified GICC05 age scale. Gaps exist in the data where sections of ice core were missing, damaged, or too small to be used. **a.**) Electrolytic conductivity is shown in µS/cm. **b.**) Dust is shown as the number of particles larger than 1 micron in diameter (see Simonsen et al., 2018 for more on Abakus measurements and particle diameter). **c.**) Ca^{2+} in ppb. **d.**) NH_4^+ in ppb. **e.**) pH in µM H^+ (shaded area indicates known calibration problems).

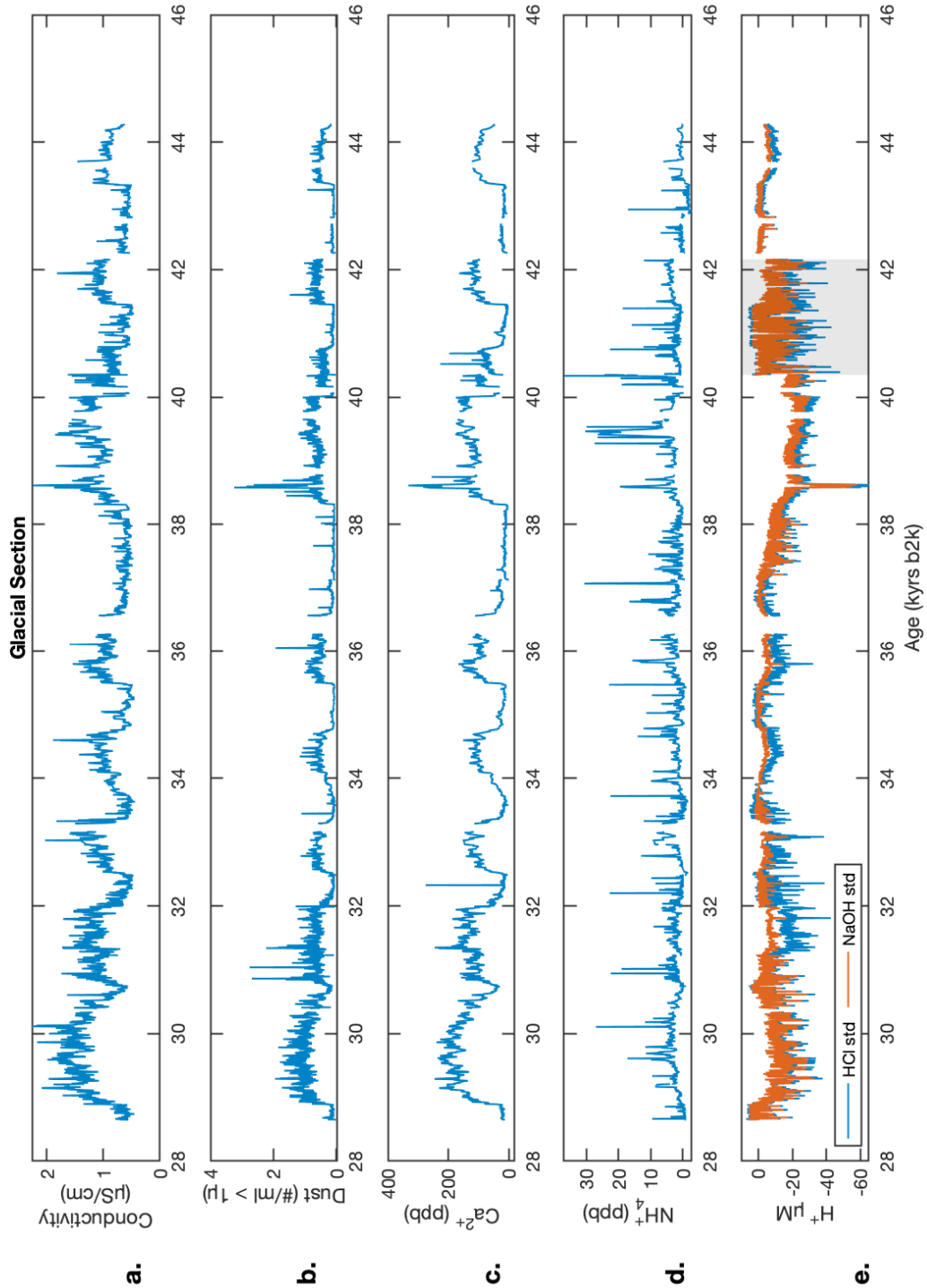

Figure 11. CFA Chemistry record for the Glacial section of Dye 3, shown here on a modified GICC05 age scale. Gaps exist in the data where sections of ice core were missing, damaged, or too small to be used. **a.**) Electrolytic conductivity is shown in µS/cm. **b.**) Dust is shown as the number of particles larger than 1 micron in diameter (see Simonsen et al., 2018 for more on Abakus measurements and particle diameter). **c.**) Ca^{2+} in ppb. **d.**) NH_4^+ in ppb. **e.**) pH in µM H^+ (shaded area indicates known calibration problems).

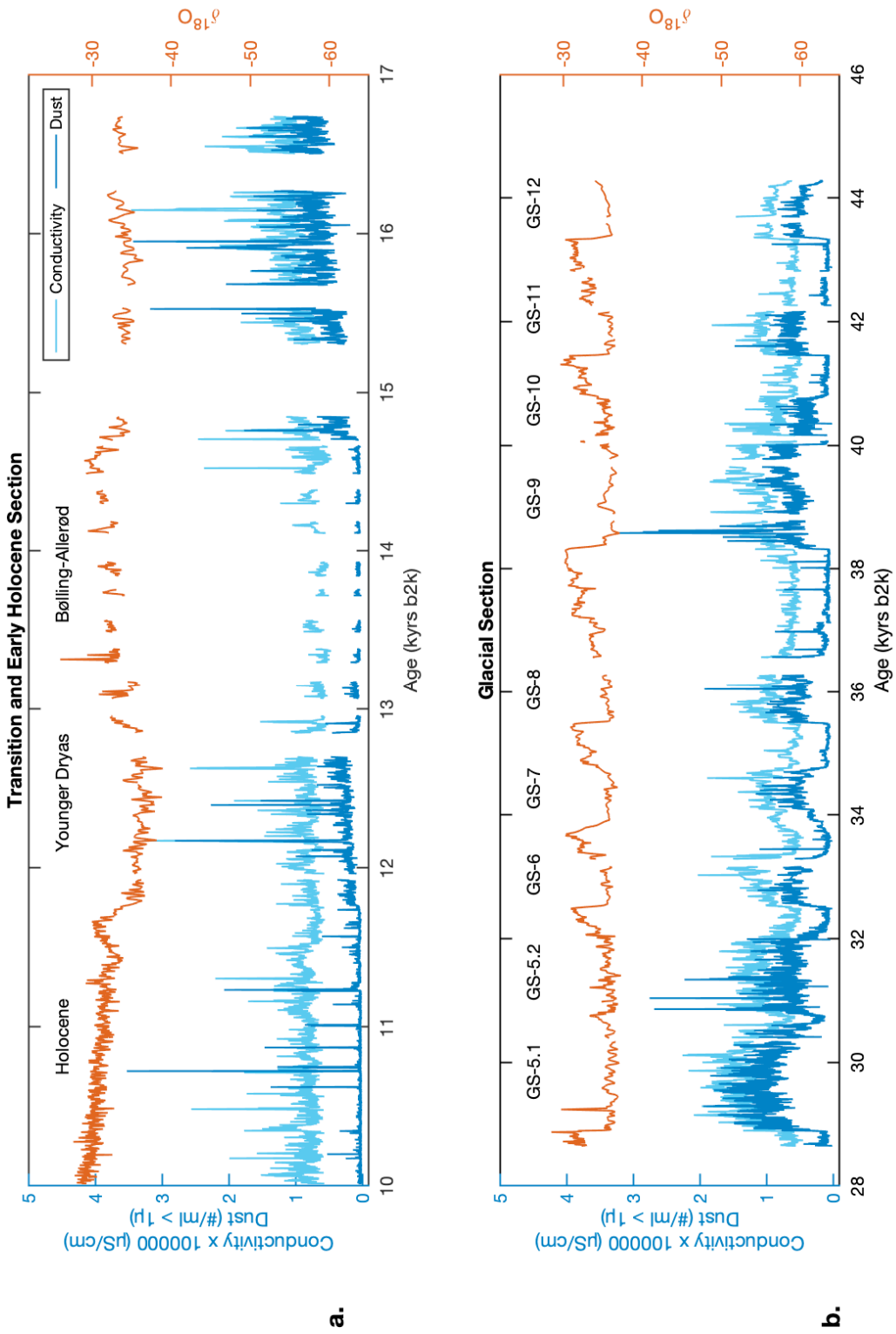

Figure 12. Dust (#/ml > 1µ) and conductivity plotted with $\delta^{18}O$ on an age scale for the Holocene (**a**) and Glacial (**b**) sections of Dye 3. $\delta^{18}O$ (‰) reproduced from (Johnsen et al., 2001). Conductivity here shown multiplied by 10,000 to compare with dust concentrations. Greenland Stadial (GS) and Greenland Interstadial (GI) numbers in accordance with Rasmussen et al. (2014).

4.2 Chemistry data

The Early Holocene and Transition section of the chemistry record produced during the CFA campaign (Figures 10) shows the timing of the Glacial transition, despite small sections of missing data throughout. The Glacial section clearly shows several Dansgaard-Oeschger (D-O) events (Greenland Stadial periods 5-12 (Rasmussen et al., 2014)). The overall profile of the record and measured impurity concentrations are as expected, based on other Greenland ice core records. The NH_4^+ record shows slight oscillations in time with the D-O events, as well as many shorter-duration peaks, possibly evidence of widespread forest fires. It is to be expected that dust, conductivity, and Ca^{2+} show very similar profiles, as insoluble particles are a significant contributor to the conductivity measurement, and much of the mineral dust that reaches Greenland contains calcium.

As there were recurrent problems during measurement, the pH record is less clear than the other impurity measurements. During the melt campaign, there was ongoing trouble with the pH instrumentation and to changes in the reagent composition throughout the campaign in an attempt to improve the pH measurements. Figures 10 and 11 indicate areas where there were known to be problems with the pH measurements or calibrations. The pH record, however is still presented here despite these problems, as it still contains valuable information.

When seen alongside the previous $\delta^{18}O$ values (Johnsen et al., 2001), the dust and conductivity results (Figure 12) again appear as expected, showing oscillation timing congruent with that shown in the previously measured $\delta^{18}O$ record. As expected, a lower $\delta^{18}O$ value, typical of periods of colder climate, tends to correspond with a higher level of conductivity and increased dust concentration. The comparison between dust, conductivity, and $\delta^{18}O$ also demonstrates that although only a preliminary age scale, the depth asignment and age scale used here are appropriate for use in this analysis.

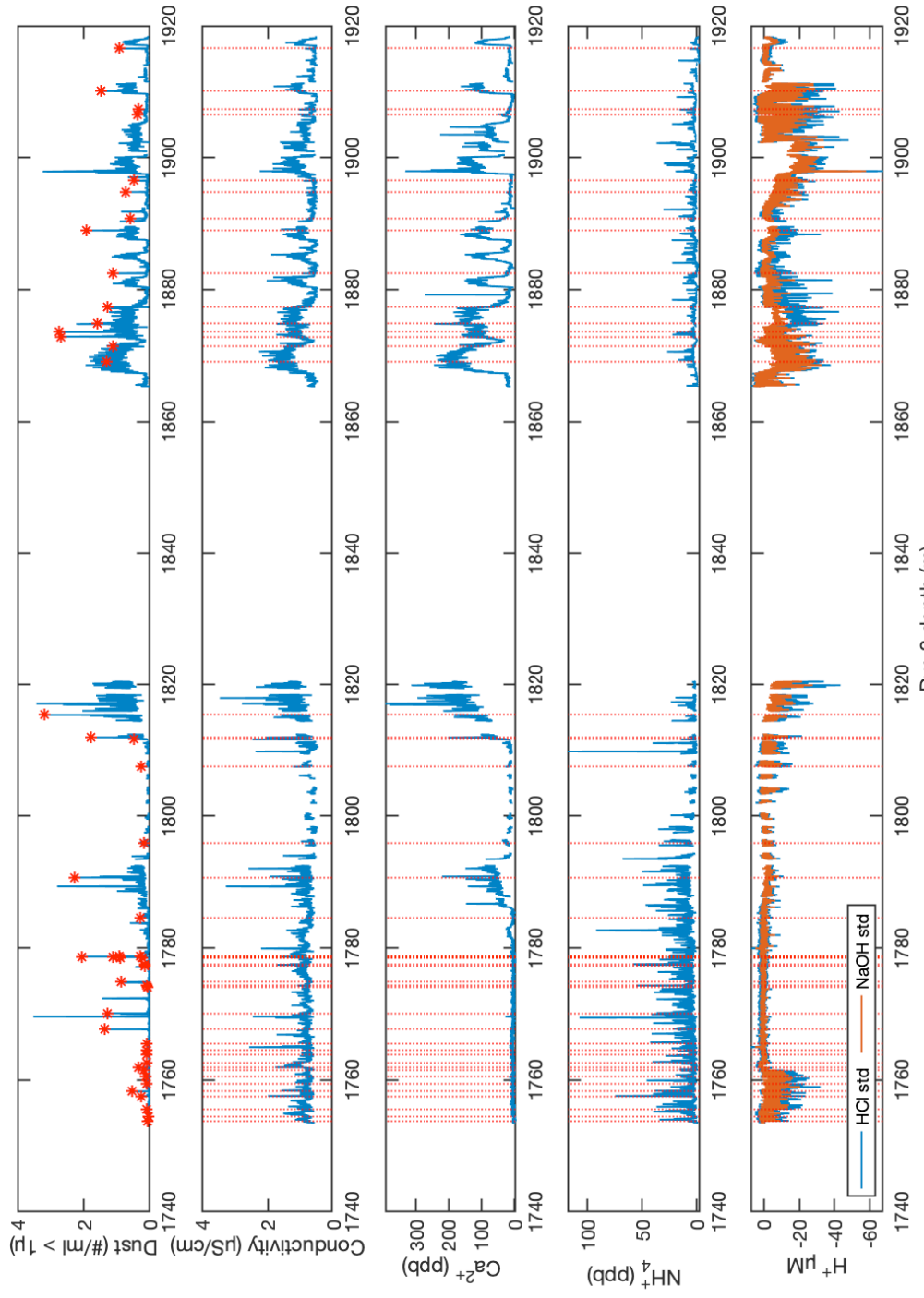

Figure 13. Possible contamination in Dye 3. **a.** Complete Dye 3 dust record plotted to depth, shown here with identified possible contamination spikes marked with a "∗". **b-e.** CFA chemistry record - dotted lines indicate the depths of flagged possible contamination spikes, as seen in the dust record.

4.3 Possible contamination

There is a risk of possible contamination each time a break in the ice passes the melt head. Therefore, it is important to present the data flagged for possible contamination spikes that coincide closely with recorded breaks (Figure 13). As the potential contamination was identified using only the dust record, the peaks resulting from possible contamination are marked. For the remaining measured species, only the depths of the dust spikes are marked, as the delay times used for the chemistry records are approximated for each run and cause slight variation in the depth assignment. It is, however, still possible to use this depth information to identify possible contamination in the other chemistry records.

It is worth noting that while there appear to be more contamination spikes in the Holocene, especially at the shallower end of the record, this is likely influenced by the fact that the Glacial period has a significantly higher range of variability, especially within the Glacial Stadials. This high variability has the potential to mask contamination spikes, making it more difficult to visually identify contamination.

The measured Dye 3 record consisted of a total of 116 "bags," with a total of 221 breaks within the bags recorded in the lab during the duration of the melt campaign. Therefore, there are approximately 337 recorded breaks in the total length of ice melted. Using the method described above, there were 48 spikes identified as possible contamination from the dust record. Therefore, contamination peaks were identified at fewer than 15 percent of all recorded breaks in the ice.

5. Discussion

5.1 Primary observations

The conductivity signal shows values within an expected range based on the analyses of other ice core records. Additionally, the conductivity appears to quite clearly show the reverse signal of the δ^{18}O record, indicating, as expected that the impurity content increases during cold periods with lower δ^{18}O values, and decreases during warmer periods with higher d18O values.

The dust record has a considerable amount of data spikes in the earlier Holocene section, however many of the dust peaks have been flagged as possible contamination (as seen in Figure 13). As the dust record simply shows the total insoluble particles in the ice (Hammer et al., 1985; Steffensen, 1997), it would be helpful to perform further analysis to find out the composition of the microparticles themselves. As microparticles have not been collected for analysis, however, the other impurity records can be used to understand the possible composition of the dust peaks. As such, Steffensen (1997) presents a good demonstration of the relationship between dust concentrations and calcium. A considerable amount of the dust in ice cores comes from calcium rich mineral sediments, including calcite ($CaCO_3$) and gypsum ($CaSO_4$). The calcium record, therefore, varies in parallel with the dust or insoluble particle record, as seen in Figures 10 and 11. Not all dust spikes are seen in the calcium record, however. Spikes that occur in dust and not calcium show that the dust spike is due to something other than increased continental dust and could indicate volcanic particulates or contamination. It is therefore important here to note possible contamination spikes that occur in proximity to a break in the ice.

Ammonium is commonly used in ice cores as a proxy for biomass burning, typically associated with forest fires, and spikes in ammonium tend to indicate large scale wildfires (Legrand et al., 2016). However they can also indicate the presence of contamination incident at a break in the ice. Figure 13 is therefore helpful in revealing which ammonium peaks are likely due to contamination and which could be signals of past forest fires. It is also possible to recognize stadial-interstadial variability in the background ammonium record, representative of the changing continental ice sheet extent.

It is apparent from the pH record that the ice from the Glacial period is slightly alkaline. In the ice covering approximately 33 to 38 kyrs b2k, oscillations in the pH signal can be seen, in opposition with the dust, calcium, and

conductivity profiles. These oscillations vary in time with the D-O events during this period. This oscillation in pH is likely due to the high concentrations of calcium rich dust, some of which reacts with strong acids in the ice, making the resulting meltwater alkaline (Steffensen, 1997). The alkalinity of the ice during colder periods is worth noting, as pH is often used as a proxy for the volcanic record. Therefore, neutralization of the volcanic acids and increased background alkalinity masks the volcanic signal, making identification of volcanic events by pH during the cold glacial period especially difficult.

Throughout the campaign, two standards are used in the calibration of the pH signal, composed of dilutions of HCl and NaOH respectively. These two standards are selected with strengths similar to the pH range found in the sample ice, as the calibrations are most appropriate when the standard's concentrations correspond with the approximate sample measurement signal. The pH signal shown in Figures 10 and 11 is determined using the two standards, and as the pH of the sample changes, it becomes more appropriate to use calibrations based on the two standards for different sections of ice. Therefore, it is suggested that the alkalinity standard, NaOH, is best used in the more alkaline glacial period, while the acidic standard, HCl, is better used for the Holocene section. Both calibrations are presented here for completeness and ease of comparison.

5.2 Variations across climatic periods

In order to compare selected Dye 3 chemistry parameters across different climatic conditions, characteristic values for the Early Holocene, Stadial, and Interstadial conditions are calculated. For the Holocene, the period of approximately 10,100 - 10,600 b2k is used here. For the Greenland Stadial (GS) and Greenland Interstadial (GI) periods, the event onsets outlined in Rasmussen et al. (2014) for Stadials 5 - 12 were used to define the stadial/interstadial transitions, with a 100 year buffer added to either side of the onset times so as not to consider the transition values. Once time periods were defined, all GS and GI values (respectively) were combined in order to calculate mean and median values for comparison.

Table 2. Summary statistics across climatic periods.

		mean	median	std dev	range
Conductivity ($\mu S/cm$)	Holocene	0.83	0.77	0.20	1.99
	Stadial	1.13	1.08	0.26	1.69
	Glacial	0.61	0.59	0.08	0.97
Dust ($\#/ml > 1\mu$)	Holocene	2959	2709	1951	52366
	Stadial	66684	60559	28246	322733
	Glacial	10352	8987	5494	86205
Calcium (ppb)	Holocene	6.56	6.50	2.66	20.57
	Stadial	119.67	113.08	40.59	314.82
	Glacial	18.67	16.54	9.89	273.91
Ammonium (ppb)	Holocene	5.86	3.70	6.92	75.83
	Stadial	3.33	2.57	3.45	37.24
	Glacial	1.04	0.73	2.24	33.43

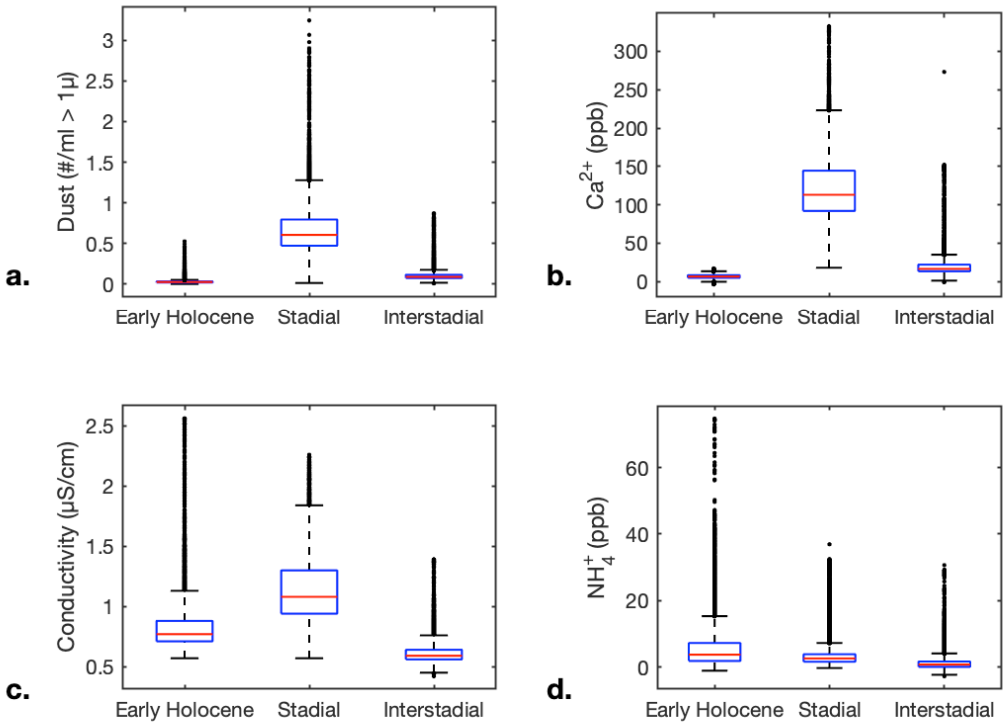

Figure 14. Box and whisker plots presenting a summary statistics comparison between observed concentrations during selected climactic periods. Red lines indicate median values, bottom and top of the boxes represent the 25th and 75th percentile (respectively), and whiskers extend to the most extreme non-outlier values. Outliers are shown with black dots. **a**. Comparison of dust concentrations (#/ml > 1µ), **b**. Ca^{2+} concentrations (ppb), **c**. electrolytic conductivity (µS/cm), and **d**. NH_4^+ (ppb) for the chosen time periods. (Calculations are made according with the "boxplot" function in MATLAB)

Using summary statistics, it is possible to make a general statistical comparison between the different climactic periods represented in the Dye 3 ice core (Table 2, Figure 14). The colder stadial periods, in all but the ammonium record, have significantly higher concentrations than both the Holocene and the Interstadial periods. Additionally, the distribution for the Stadial periods is much wider, indicating that the climate was not only colder, but likely also much more variable during the stadial periods.

Unsurprisingly, there are again similarities between the dust, conductivity, and calcium, with calcium and dust the most similarity. Dust, conductivity, and calcium all display low values during the warmer Holocene and interstadial climate periods and higher values during the cold Glacial stadial period. The ammonium record shows higher variability and significantly more outlier values in the Holocene. It is likely that this is due to the increased boreal fire activity during the Holocene, as the large continental ice sheets receded, exposing more area susceptible to biomass burning. It is important to note here, as mentioned earlier, that as no data was removed from the record due to the assumption of contamination. It is therefore likely that some of the outlier data in this analysis is actually a result of contamination.

5.3 Comparison to previous Dye 3 records

As the Dye 3 ice core was drilled in 1979-81 and has been the subject of multiple analyses, it is appropriate to begin by comparing the recent data here with the results from previous studies. Dye 3 and insoluble particle measurements were the subject of the 1995 PhD. thesis written by J.P. Steffensen, which is a valuable source for data to make comparisons. Sicne 1995, there have been changes and improvements to the methodology used. The data presented in Steffensen (1995) was obtained as discrete measurements, sampled using a coulter counter for insoluble particles, and ion chromatography for the ionic species. Due to the differences in measurement techniques, it is expected that there should be differences between the results.

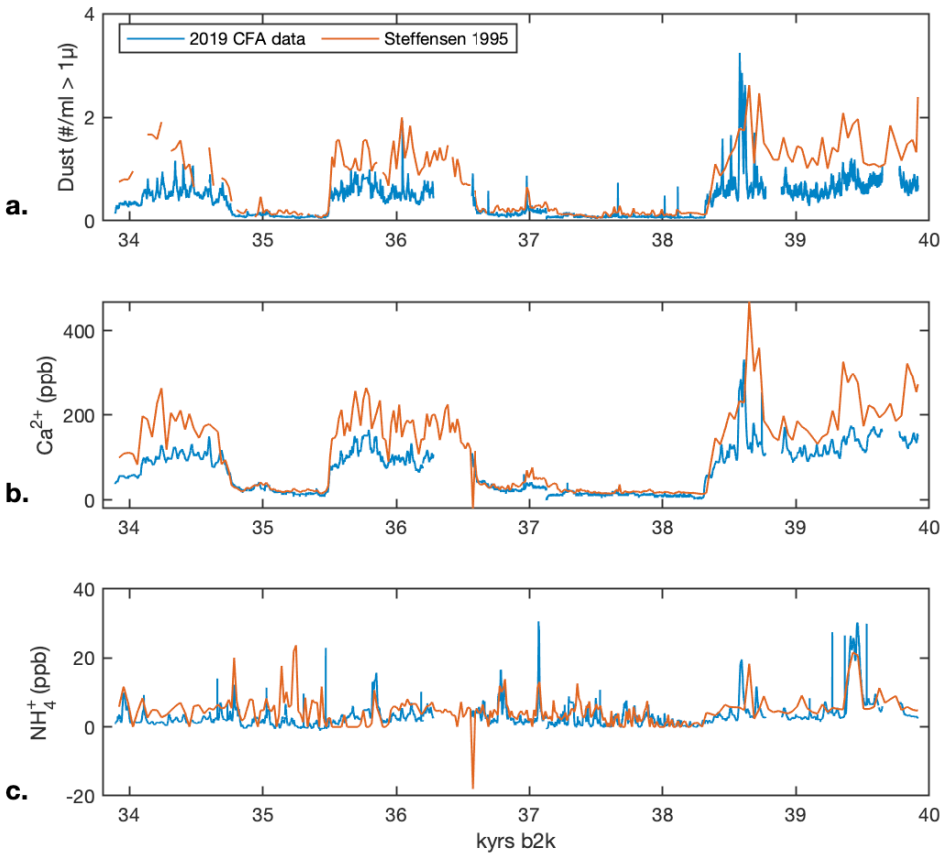

Figure 15. Comparison plot of recent Dye 3 data with data from the PhD. thesis of J.P. Steffensen, 1995. **a.** Dust particles larger than 1 micron in diameter (#/ml > 1μ). Note that the Steffensen, 1995 data was collected using a Coulter counter, and thus some difference between the results is expected. **b.** Calcium, shown in parts per billion. **c.** Ammonium, shown in parts per billion. Note that the Steffensen, 1995 data was collected using ion chromatography, and converted from μequivalents/kg. All plots shown relative to the interpolated age scale, discussed previously in section 4.1.

The Glacial section data are quite consistent between the 1995 measurements and the present CFA data in terms of D-O event variability. The dust signal exhibits the same variation in both data sets, the stadial-interstadial pattern is well represented, and the D-O event transitions are clearly defined. Both data sets show significantly higher dust quantities as well as higher levels of variability during the cold stadial periods as compared with the warmer interstadial periods. This trend is also replicated in the Calcium signal. In both cases, the absolute levels are higher in the Steffensen (1995) data, especially during the stadials, where values are nearly nearly a factor of two higher. However, due to the differences in resolution, instrumentation, and measurement technique it is

difficult to precisely attribute cause.

At approximately 38.6 kyrs b2k, there is a significant peak in all species shown here in both Dye 3 records. This peak is not seen to the same degree in other Greenland ice core locations, and is not known to be related to any known volcanic event. It could be the signal of some yet unknown feature in the ice record, It is also not in close enough proximity to an identified break to be classified as contamination, however, it could be due to a some refrozen breake or other contamination inclusion in the ice. It is unlikely, however, that the continuous measurements from 2019 and the discrete measurements from 1995 would both show the same contamination, since the sample decontamination processes were not the same during both measurements. Further investigation into the source of this signal is warranted.

Although the D-O event signal is not present in the ammonium record, most of the notable spikes in the ammonium signal are seen in both the present and the 1995 data. The similarities seen in both sets of data are useful, both in confirming the appropriateness of the depth scale created in this analysis (as described previously) and in indicating that there has not been significant deterioration of the ice core during the period in storage.

The differences resulting from the use of an Abakus and a Coulter Counter was thoroughly investigated in Simonsen et al. (2018). The most significant discrepancy between the Abakus and Coulter Counter is due to the irregularity of particle shape, and thus particle size characterization. For the purpose of comparing dust concentrations, however, the Abakus and Coulter counter should be somewhat similar, except in cases in which the size is incorrectly characterized as larger or smaller than 1 micron. 1 micron is the diameter at which the background noise begins to overwhelm the signal for smaller particles measured with the Abakus and thus the minimum particle size cutoff used here. If particles are differently characterized relative to this 1 micron cutoff value, significant differences in dust concentrations could be seen.

For the ionic species as well (calcium and ammonium), differences in measurement methods must be considered. While the recent CFA data results were obtained using absorption and fluorescence methods, in ppb concentrations, the 1995 data results from ion chromatography (IC) measurements, measurement of ions in solution independent of the compounds from which they originate, given in µequivalents H^+ per kg of ice. In order to make a comparison between the two quantities, a simple conversion factor is used, based on the atomic weight of the ions in question. Additionally, the measurement methodology may also impact the

measured ionic concentrations. The CFA measurements are performed immediately after the ice sample is melted, while the IC process takes considerably longer, and the samples are melted relatively earlier prior to analysis. For the calcium measurements, therefore, it is possible that some of the microparticles are able to dissolve in the melted sample, causing an increased calcium signal to be seen. This difference between the two measurement types must be noted, as it has an impact on the ability to make a direct comparison of the results.

5.4 Comparison to other sites in Greenland (NEEM and NGRIP)

The ability to compare ice core records from different locations across Greenland is key to understanding the glaciology of Greenland, as well as the differences in climate conditions across the ice sheet. This section presents a comparison of the present Dye 3 data to similar CFA chemistry records from the North Greenland Eemian Ice Drilling ice core (NEEM) (Schüpbach et al., 2018) and the North Greenland Ice Core Project (NGRIP) (Bigler, 2004; Ruth et al., 2003).

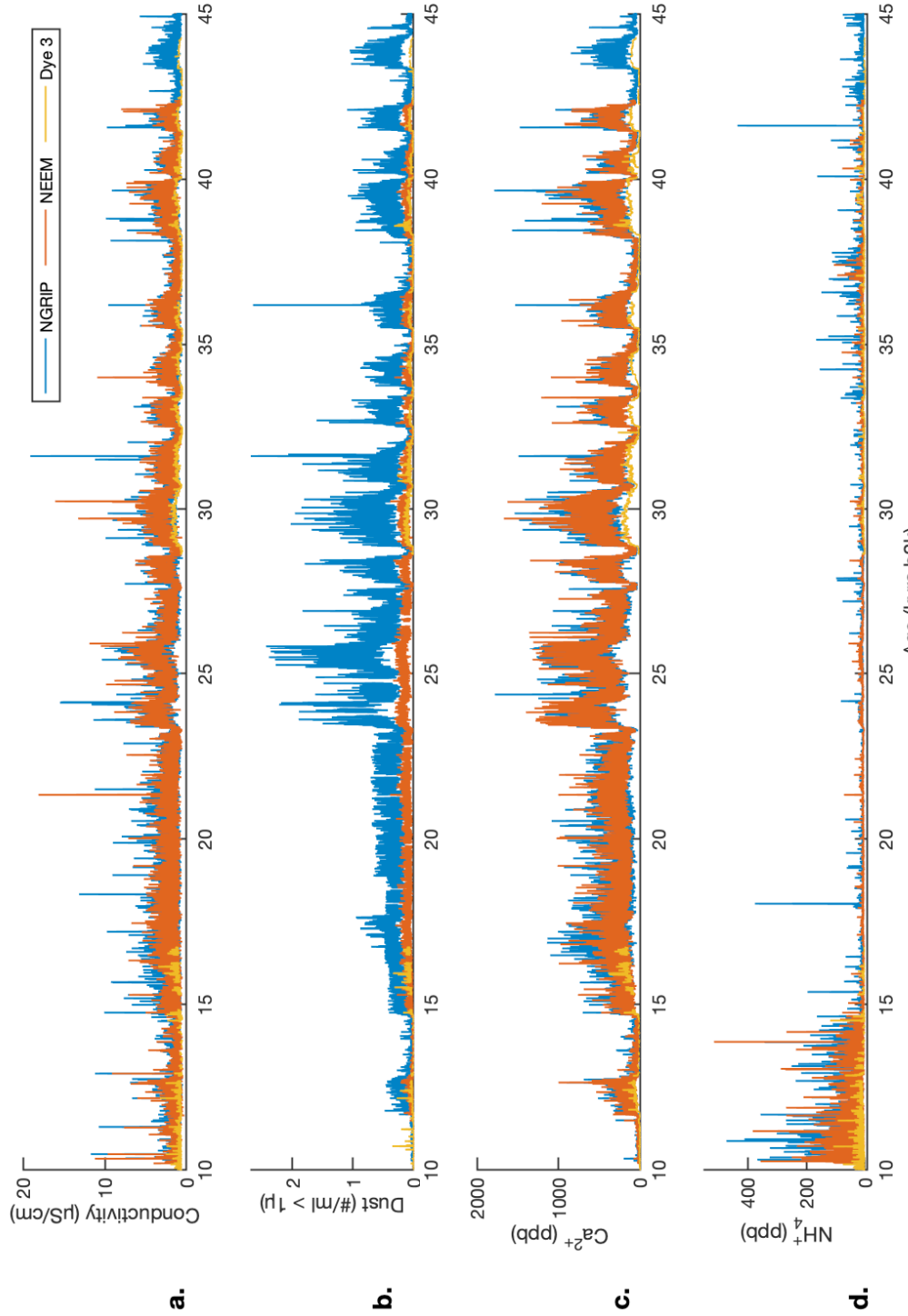

Figure 16. Conductivity (**a**), dust (**b**), calcium (**c**), and ammonium (**d**) concentration records from Dye 3, shown together with the NGRIP and NEEM impurity records, shown on the common GICC05 timescale. (NEEM and NGRIP data reproduced from Ruth et al. (2003), Bigler (2004), and Schüpbach et al. (2018).

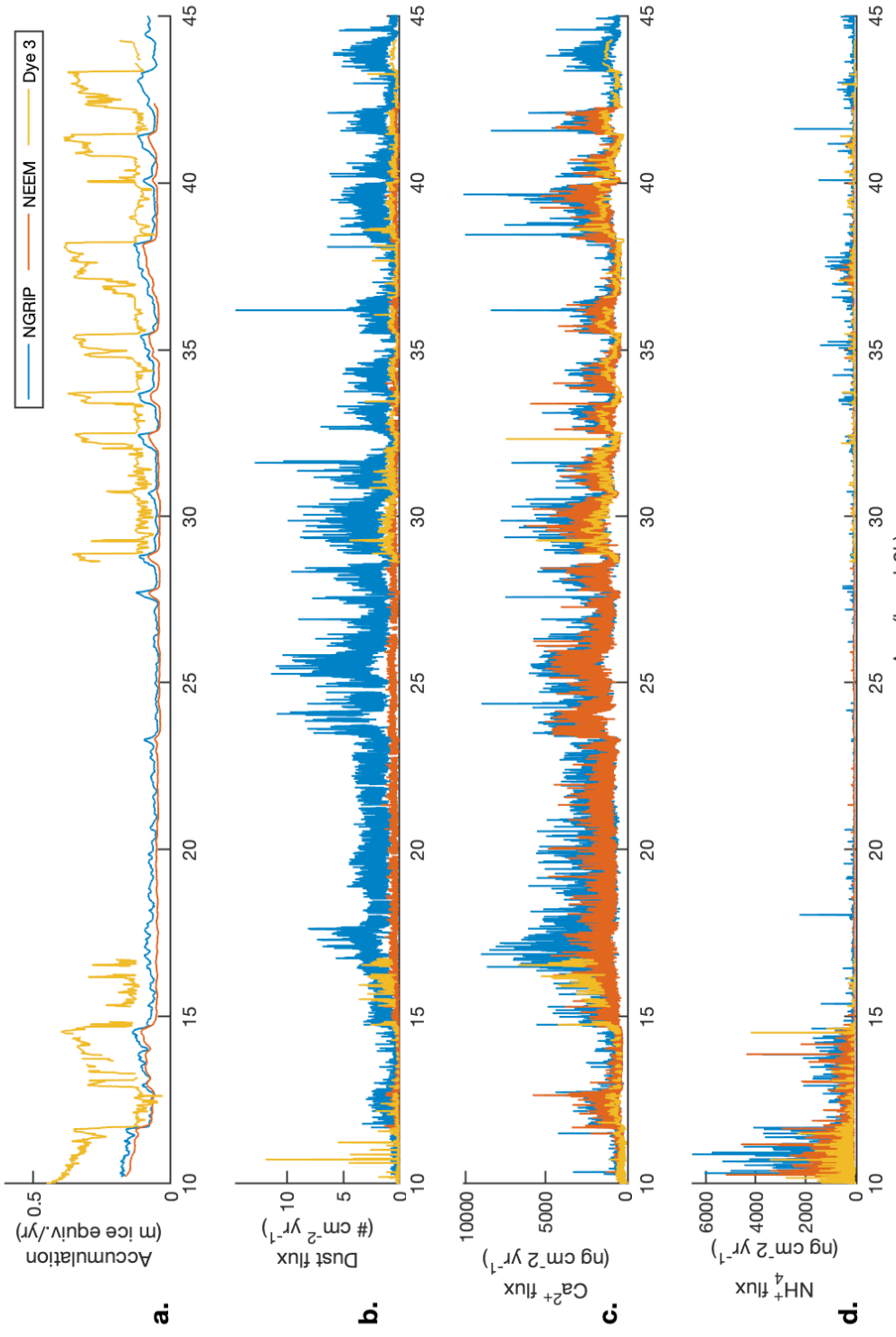

Figure 17. Accumulation rate (**a**), dust concentration (**b**), and dust and chemistry flux (**c & d**) for Dye 3, NEEM, and NGRIP, shown on the common GICC05 timescale. (NEEM and NGRIP data reproduced from Ruth et al. (2003), Bigler (2004), and Schüpbach et al. (2018); NGRIP accumulation model reproduced from Andersen et al. (2006); NEEM accumulation model reproduced from Rasmussen et al. (2013); Dye 3 accumulation model provided by Bo Vinther (unpublished - personal correspondence, 2020)).

The Dye 3 data are shown together with the NEEM and NGRIP records (Figure 16). While the conductivity record for NEEM and NGRIP are quite similar, both in scale and in variability, the Dye 3 conductivity values are much lower overall, during the Holocene, Transition, and Glacial periods. Although a similar pattern is seen in the calcium and ammonium records (similar concentrations seen in NEEM and NGRIP, while Dye 3 has lower concentrations overall), it is somewhat unexpected that the same pattern is not found in the dust concentrations. The dust levels of Dye 3 and NEEM mimic those seen in the conductivity and calcium, however NGRIP shows significantly higher dust concentrations than both NEEM and Dye 3. During measurement of microparticles in NGRIP, however, the sample stream from the Glacial section (ice below 1494.9 meters depth, or from the Younger Dryas and earlier) was diluted due to high dust volume. The data from the diluted sample measurements were calibrated separately, and it is possible that this dilution or calibration had some impact on the measured dust concentrations (Ruth et al., 2003).

Understanding the implications of these comparisons requires knowledge of the climatic conditions at each of the different sites. The low impurity concentrations in the Dye 3 record are not unexpected, due to the fact that the Southern Greenland location of Dye 3 means it has significantly higher accumulation rates than the more Northern NEEM and NGRIP. It is likewise important to understand the mechanisms through which these different compounds end up in the ice. Typically, atmospheric aerosols are deposited on the snow surface through a combination of wet and dry deposition (Bergin et al., 1995; Fischer et al., 2015; Schüpbach et al., 2018). Both types of deposition play a role in the accumulation of impurities in glacial ice, and both Fischer et al. (2015) and Schüpbach et al. (2018) present and utilize a deposition model to reconstruct atmospheric composition of both the atmosphere over the ice sheet and at the source of the impurities. Bergin et al. (1995) investigates the relative importance of different types of impurity deposition (dry fallout, wet deposition via snowfall, and fog deposition), and show that wet deposition via snow plays a primary role in accumulation of chemical species in glacial ice. Additionally, for dust particles, particularly those with a radius smaller than 10 microns, wet precipitation is the dominating deposition mechanism (Steffensen, 1995). Therefore, understanding the accumulation differences in accumulation rate for the different sites is crucial to making sense of the impurity record.

The impurity concentrations are multiplied by the accumulation rates (model reconstructions) to determine the impurity flux (Figure 17), which, when

viewed alongside the absolute concentrations (Figure 16), gives insight into the how the different conditions of the ice core sites can manifest in the impurity record. As flux is the product of the accumulation rate (which is measured in meters of ice equivalent per year) and the impurity concentrations (given in ppb or particles per milliliter, both relative to ice core meltwater), some care must be taken with the units. The density of Glacial ice, 917 kg/m^3, must be taken into account when converting the accumulation rate from ice equivalent into water equivalent, and as a common unit for flux is nanograms per year per square centimeter of ice surface (ng cm$^-$2 yr^{-1}), the accumulation rate must be multiplied by 91.7 (kg/(m$*$cm^2)) in order to obtain the appropriate units.

Accumulation models for the NGRIP (Andersen et al., 2006), NEEM (Rasmussen et al., 2013), and Dye 3 (Vinther, 2020 – personal correspondence) were used to produce flux estimates as described above (Figure 17). When corrected for the difference in accumulation, the Dye 3 impurity flux is much closer to that of both NEEM and NGRIP, with the exception of dust. The same signals can be seen in the three cores with respect to major climatic events and their timing, indicating that, for the presented record, the different locations atmospheric aerosol concentrations are relatively similar, yet impacted by the differences in accumulation.

Table 3. Stadial:Interstadial ratio of impurities content for Dye 3 (2020 and 1995 data), NEEM, and NGRIP ice cores.

	Dye 3 (2020)	NEEM	NGRIP	Dye 3 (1995)
Conductivity	1.83	2.10	2.08	-
Dust	6.74	7.99	7.71	8.35
Dust flux	2.47	4.93	4.38	-
Calcium	6.83	5.70	6.12	8.43
Calcium flux	2.49	3.41	3.47	-
Ammonium	3.51	2.39	1.83	1.50
Ammonium flux	1.31	1.45	1.07	-

It is also useful to compare the differences between the stadial and interstadial conditions from each of the ice cores. Table 3 shows the ratio of the median stadial to median interstadial values for each of the impurity records. For conductivity, ammonium, and calcium (in both absolute concentration and flux), the stadial:interstadial ratio is considerably higher for both NEEM and NGRIP than for the 2019 Dye 3 data, The 1995 Dye 3 stadial:interstadial ratio is higher still. However, as discussed previously, this difference is possibly due to

measurement differences. The higher stadial:interstadial ratio seen in NEEM and NGRIP could indicate a higher sensitivity to the climatic variations due to their more extreme northern locations in Greenland. The ammonium does not show such a trend based on location, although the higher ratio in ammonium concentrations for Dye 3 may be related to the southern location and proximity to terrestrial biogenic ammonium sources.

5.5 Particle size distribution

In addition to the chemistry of the ice impurities, much can be gained through studying the size distribution of the particles found in the ice. The Abakus instrument for laser particle measurement determines not only the number of particles, but also the counts of particles in a number of different size bins. The size bins used are not totally comprehensive (only particles between 1 and 15 microns are measured here), but this size distribution can contain valuable information about the ice impurity record. The particle size bins used in the Abakus settings are not all the same size, however, so the data must be normalized by the size of the bin in order to more accurately represent the number of particles of each size.

Many previous studies have looked into the size distributions of the microparticles in glacial ice (Hammer et al. (1985), Steffensen (1995, 1997), Ruth et al. (2003), Simonsen et al. (2019), among others). This section presents preliminary explorations into uses for the particle size distribution from the ice core record. This is not intended to be a finalized methodology or a presentation of definitive results, but a description of investigations made into possible uses for straightforward examination of the particle size record.

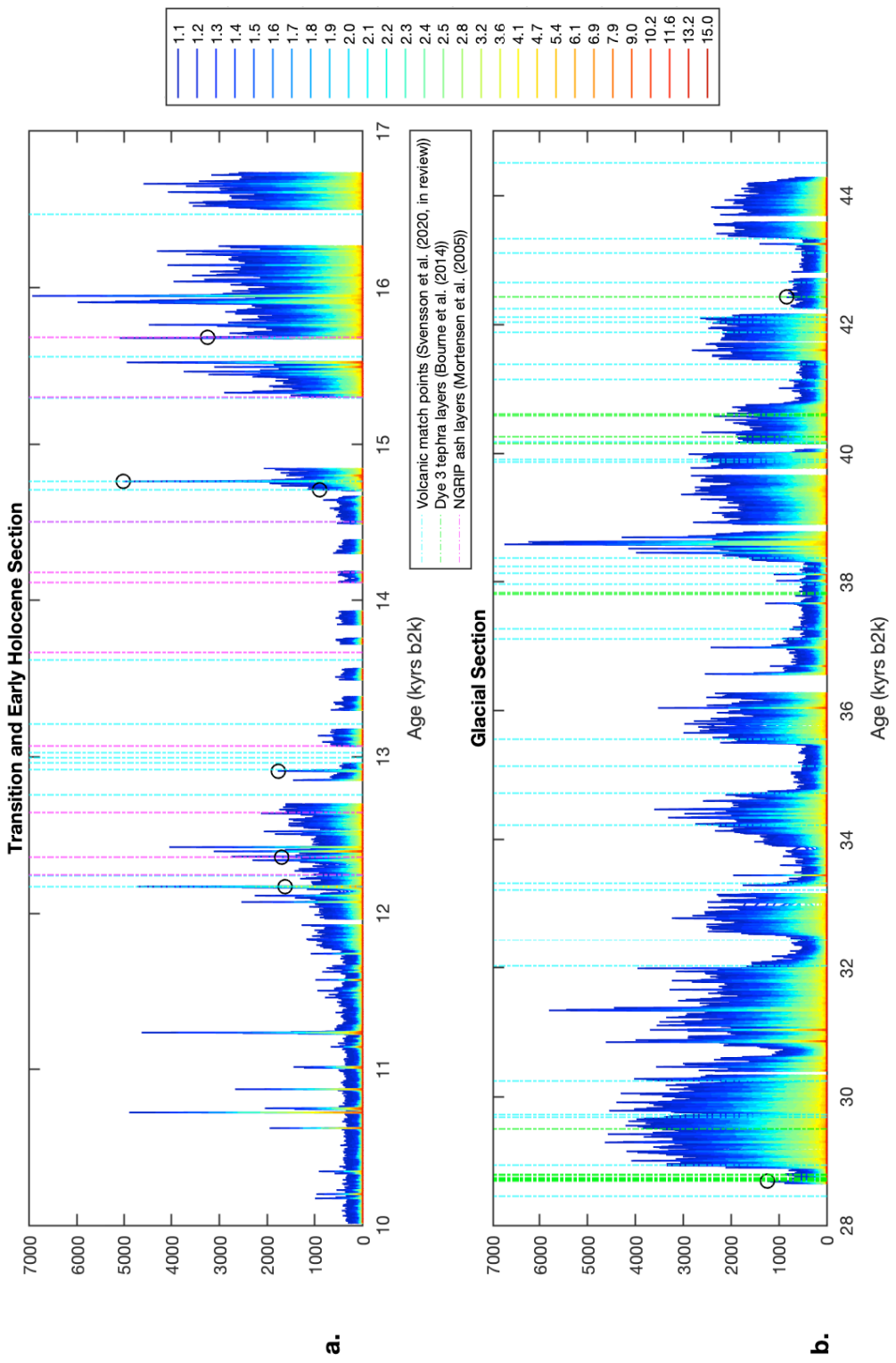

Figure 18. Particle size distribution for the (**a**) Holocene and Transition and (**b**) Glacial sections of Dye 3. Abakus dust data, shown binned by particle size (see legend). Vertical lines indicate Volcanic match points from Svensson et al. (2020); ash layers found in the Glacial Transition section of NGRIP (shown here with respect to their GICC05 age) from Mortensen et al. (2005); and tephra layers found in Dye 3 from Bourne et al. (2014), shown here converted from the given depths using the modified GICC05 scale (as used throughout this document). Non-contamination dust peaks that correspond with identified volcanic layers are marked with black circles (see detail Figure 19).

Figure 18 presents the dust record for the measured length of the Dye 3 ice core, with the contributions of the total dust concentration divided into individual curves for each particle size bin measured by the Abakus instrument (bin sizes are shown in the Figure legend). It is clear from this visualization that smaller particles dominate, and the quantities decrease with increasing particle size.

An interesting possible employment of the particle size distribution of the microparticle record is the potential for finding volcanic events or tephra layers in the stratigraphy. To this end, it is helpful to use previously identified volcanic events in the ice and attempt to classify them based on their appearance, with the hope to be able to use this to identify other volcanic events. Figure 18 also identifies known volcanic layers. The following known volcanic layers are presented here: Bipolar volcanic match points (Svensson et al., 2020) are shown respective to the GICC05 ages to which they correlate (note that as these volcanic events are bipolar, they are not necessarily in close enough proximity to the Dye 3 site that volcanic particles would be seen in the record). Volcanic tephra layers found in Dye 3 are plotted based on the depth at which they were measured, here converted to ages using the same modified GICC05 timescale used throughout (Bourne et al., 2014). As there were no tephra layers identified in the Holocene and Transition section by Bourne et al. (2014), ash layers found in the Glacial Termination section at NGRIP are shown here as well, with the given NGRIP depths converted to GICC05 ages (Mortensen et al., 2005).

There are, somewhat surprisingly, few dust spikes in the Dye 3 record that coincide with the volcanic layers identified from the sources listed above. The most significant and clearly seen of these volcanic spikes is the Vedde Ash layer, found in the Dye 3 record at approximately 1789.33 meters depth, which appears at 12,170 years b2k (on the modified GICC05 age scale used here). As shown in Figure 19a, the elevated dust event of the Vedde Ash layer spans more than a decade, with multiple peaks. Figure 19b shows a spike in the dust content at approximately 12,915 years b2k in the Dye 3 record, coinciding with the volcanic match point at 12,917 years b2k GICC05 (Svensson et al., 2020). Similar to Vedde Ash, this event spans multiple years, and shows multiple peaks in the dust concentrations. Based on the profiles of these two volcanic layers, an additional spike at approximately 10,745 years b2k is identified, shown in Figure 19. While this dust peak is much shorter in duration, it has a similar shape to those in Figure 19 a and b with multiple peaks, in addition to a considerable amount of large particles. Differences seen in Figure 19a, b, and c, may also be attributable

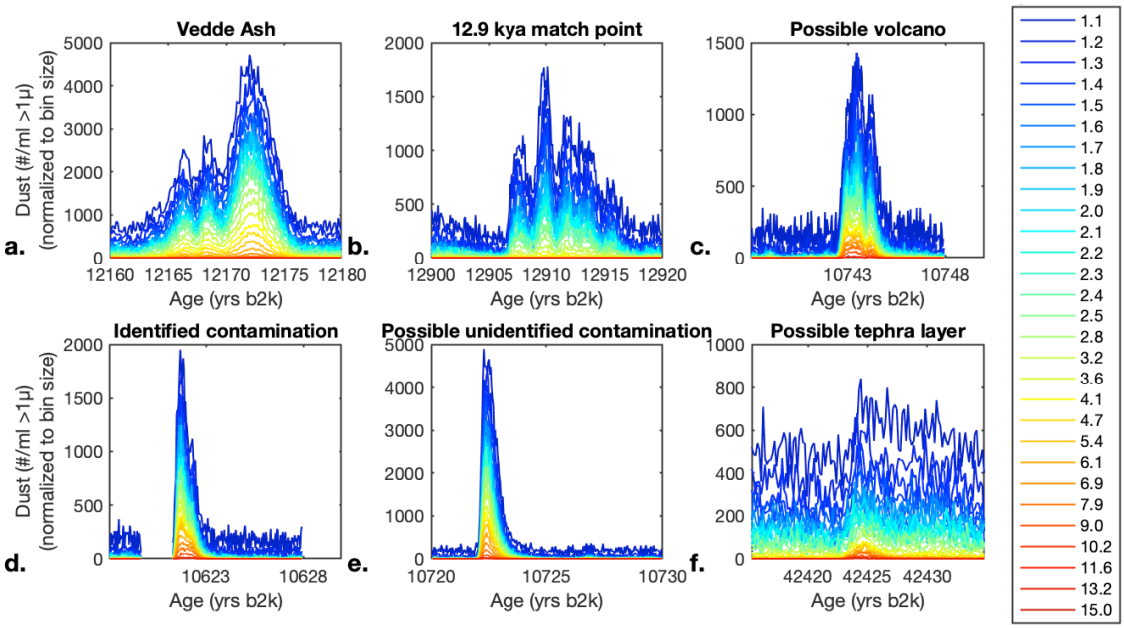

Figure 19. Selected Dye 3 dust size distribution details. Abakus dust data, shown binned by particle size (see legend). **a.** Vedde Ash layer. **b.** Possible volcanic layer identified from the 12,917 yr b2k volcanic match point (Svensson et al., 2020). **c.** Unknown dust spike with profile similar to that of the volcanic events in a & b. **d.** Contamination spike caused by a break in the ice, visually identified (note missing data at break depth). **e.** Possible contamination visually identified by apprearance, no local break in the ice or other identified contamination source. **f.** Spike in large particle quantity with no identified contamination source, coincident with the Dye 3 tephra layer described Bourne et al. (2014) at 1912.25 m depth.

to the distance of the volcano from the drill site. As large particles are less easily carried by winds, it is possible that the peak shown in Figure 19c is due to a smaller eruption closer in proximity to Southern Greenland.

In addition to the handful of spikes in the dust record that coincide with volcanic layers, many of the significant dust spikes are due to contamination of the ice sample, likely due to ice core drilling fluid entering in the sample stream at breaks in the ice. Figure 19d shows the size distribution of a spike in the dust record that is likely caused by contamination at a break in the ice at 1790.64 depth (note the missing data, indicating ice was removed). This spike has a characteristic shape that is very different from the spikes seen in ether Figure 19a, b, or c, which are thought to be volcanic events. As the ice is melted from top to bottom (from shallow to deep within the ice sheet), the profile of this spike exhibits a very sharp increase in the concentration of microparticles of all sizes, including the largest particle sizes, followed by a more gradual decrease. Because the ice is melted

backwards in time, this profile would not be expected to occur naturally, as it seems quite unlikely that there would be such a sudden decrease in atmospheric microparticles. This profile, seemingly characteristic of contamination, can be used as a way to screen data for potential contamination, especially at locations where there is not an identified break in the ice to otherwise aid with the identification of possible contamination. As such, Figure 19e shows the dust profile of a spike that occurs at a location where there is no proximity to any recorded break. This profile closely resembles that of a contamination spike, leading to the belief that it is evidence of contamination. This could be, for example, due to a failure to properly record the break, misalignment of the ice on the melt-head, or a refrozen break.

Ideally, the particle size distribution data would be useable for finding tephra particles within the ice. At present, tephra can be quite difficult to find, relying on sulfate data or extensive previous investigations into the ice core records, analyzed by optical microscopy as well as electron probe microanalysis (Bourne et al., 2014). As tephra particles are typically considerably larger than windblown dust particles (Dye 3 tephra identified in Bourne et al. (2014) measure between 22.5 and 137.5 microns), it would make sense that locations within the ice with higher quantities of large particles could possibly indicate the presence of tephra. Figure 19f shows a detail of the particle size distribution centered around the tephra layer identified in Dye 3 by Bourne, et al. (2014) at 1912.25 m depth, likely from the Grimsvötn volcano. It is clearly visible that there is an increase in larger particles. It is worth noting, however that in the tephra analysis, Bourne et al. (2014) found four tephra shards found in this sample, between 37.5 and 70.0 microns in size and the Abakus bin sizing for this Dye 3 analysis has a maximum measured particle size of 15 microns. It could be possible, however to adjust the Abakus settings to better identify large particles that might be indicative of the presence of tephra.

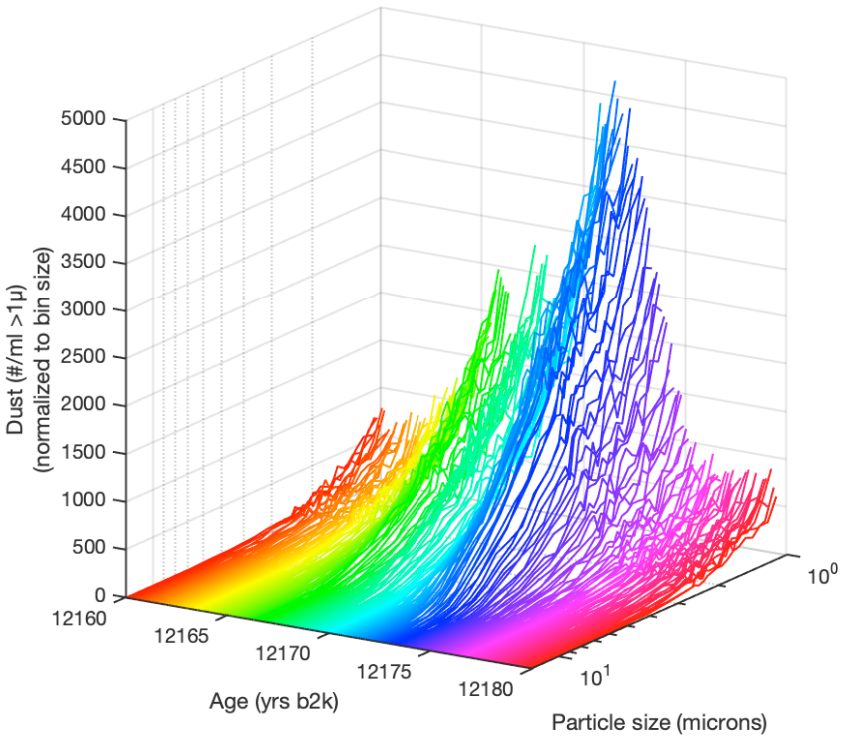

Figure 20. Evolution of the particle size distribution over time for the Vedde Ash layer. Each line indicates a size distribution measurement point as measured by the Abakus (colors chosen for ease of data visualization).

In order to present the microparticle size profile in a novel and meaningful way, it is possible to plot the size distribution data as a 3D visualization of the particle concentration of each size over time (figure 20). In this way, it is possible to more clearly see the evolution of the particle size distribution over time throughout the course of a volcanic event record, such as the Vedde Ash layer. The Vedde Ash layer has an interesting profile in Dye 3, not seen in the NEEM or NGRIP dust records, comprising a large microparticle peak lasting approximately six years, followed by two smaller peaks, lasting approximately three years each. It is clear from figure 20, as well, that all three peaks show a significantly increased concentration of larger particles.

6. Conclusion

This project presents the ice chemistry and impurity results of a high resolution continuous flow analysis campaign on the Dye 3 ice core. The Dye 3 ice core, recovered in 1981, while the subject of many analyses in the immediate years following its drilling, has sat in archival freezer storage for nearly forty years. Despite this, the Dye 3 ice remained a valuable untapped source of important climatological information, waiting to be the studied using some of the many new techniques in ice core science developed since its drilling. As a joint project investigating multiple different characteristics and climate proxies, this report includes only a fraction of the wealth of data created during the duration of the campaign.

As this is not the first impurity record from Dye 3, a comparison to previous Dye 3 data has proved useful in corroborating the data, confirming findings from previous analyses, and offering a higher resolution record to present alongside previous discrete analyses. Additionally, as Dye 3 is one one the earliest of the many ice cores drilled in Greenland, and is unique in its southern location, a comparison to two subsequent ice cores (NEEM and NGRIP) shows results comparable with expectations due to the known characteristics and conditions of the ice core sites.

6.1 Outlook

The primary investigation into the potential usefulness of a continuous microparticle size distribution record along the length of an ice core shows promise. The potential for identifying possible tephra layers, finding previously unknown inclusions of contamination in the data, and for better understanding the size distribution characteristics seen in known volcanic layers are all uses for size distriburion to be explored further. This type of analysis, therefore, is a valuable tool in the study of ice cores, and warrants further exploration. Additionally, it may be possible to use the ratio of large to small particles in order to systematically scan the data for potential volcanic events to efficiently direct further search for tephra layers.

Finally, this CFA record represents only a fraction of the data collected in the 2019 Dye 3 campaign. It would, therefore, be a great advantage to look into the way all of the data comes together to present a more complete picture of the climate record contained in this ice core. The water isotope and the atmospheric

gas measurements taken alongside the chemistry in this campaign are sure to add a great deal to our understanding of the chemistry and microparticle impurity data presented here.

References

Andersen, K. et al. (2006). "The Greenland Ice Core Chronology 2005, 15-42 ka. Part 1: constructing the time scale". In: *Quaternary Science Reviews* 25.23-24, pp. 3246–3257. ISSN: 02773791. DOI: 10.1016/j.quascirev.2006.08.002.

Bergin, M. H. et al. (Aug. 1995). "The contributions of snow, fog, and dry deposition to the summer flux of anions and cations at Summit, Greenland". In: *Journal of Geophysical Research: Atmospheres* 100.D8, pp. 16275–16288. ISSN: 0148-0227. DOI: 10.1029/95JD01267. URL: https://doi.org/10.1029/95JD01267.

Bigler, M. (2004). "Hochauflösende Spurenstoffmessungen an polaren Eisbohrkernen: Glazio-chemische und klimatische Prozessstudien". PhD thesis. Physics Institute, University of Bern, Switzerland.

Bigler, M. et al. (2011). "Optimization of high-resolution continuous flow analysis for transient climate signals in ice cores". In: *Environmental Science and Technology* 45.10, pp. 4483–4489. ISSN: 0013936X. DOI: 10.1021/es200118j.

Biscaye, P. E. et al. (1997). "Asian provenance of glacial dust (stage 2) in the Greenland Ice Sheet Project 2 Ice Core, Summit, Greenland". In: *Journal of Geophysical Research: Oceans* 102.C12, pp. 26765–26781. ISSN: 21699291. DOI: 10.1029/97JC01249.

Bourne, A. J. et al. (2014). "A tephra lattice for Greenland and a reconstruction of volcanic events spanning 25-45 ka b2k". In: *Quaternary Science Reviews* 118, pp. 122–141. ISSN: 02773791. DOI: 10.1016/j.quascirev.2014.07.017. URL: http://dx.doi.org/10.1016/j.quascirev.2014.07.017.

Bradley, R. S. (2015). *Paleoclimatology*, pp. 341–348. DOI: 10.1016/B978-0-12-386913-5.00005-3.

Dansgaard, W. (2004). *Frozen Annals - Greenland Ice Sheet Research*. Ed. by Physics The Department of Geophysics of The Neils Bohr Institute for Astronomy and Denmark Geophysics at the University of Copenhagen. The Neils Bohr Institute, p. 124. ISBN: 8799007800.

Dansgaard, W. et al. (1982). "A New Greenland Deep Ice Core". In: *Science* 218.4579, pp. 1273–1277. ISSN: 19457197.

Dansgaard, W. et al. (Jan. 1985). *Dating and Climatic Interpretation of Two Deep Greenland Ice Cores*. DOI: doi:10.1029/GM033p0071. URL: https://doi.org/10.1029/GM033p0071.

Fischer, H. et al. (2007). "Glacial/interglacial changes in mineral dust and sea-salt records in polar ice cores: Sources, transport, and deposition". In: *Reviews of Geophysics* 45.1, pp. 1–26. ISSN: 87551209. DOI: 10.1029/2005RG000192.

Fischer, H. et al. (2015). "Millennial changes in North American wildfire and soil activity over the last glacial cycle". In: *Nature Geoscience* 8.9, pp. 723–727. ISSN: 17520908. DOI: 10.1038/ngeo2495.

Hammer, C. U. et al. (Jan. 1985). *Continuous Impurity Analysis Along the Dye 3 Deep Core*. DOI: doi:10.1029/GM033p0090. URL: https://doi.org/10.1029/GM033p0090.

Herron, M. and C. C Langway Jr. (Jan. 1985). *Chloride, Nitrate, and Sulfate in the Dye 3 and Camp Century, Greenland Ice Cores*. DOI: doi:10.1029/GM033p0077. URL: https://doi.org/10.1029/GM033p0077.

Johnsen, S. et al. (2001). "Oxygen isotope and palaeotemperature records from six Greenland ice-core stations: Camp Century, Dye-3, GRIP, GISP2, Renland and NorthGRIP". In: *Journal of Quaternary Science* 16.4, pp. 299–307. ISSN: 02678179. DOI: 10.1002/jqs.622.

Kaufmann, P. et al. (2008). "An improved continuous flow analysis system for high-resolution field measurements on ice cores". In: *Environmental Science and Technology* 42.21, pp. 8044–8050. ISSN: 0013936X. DOI: 10.1021/es8007722.

Kjær, H. A. et al. (Oct. 2016). "An Optical Dye Method for Continuous Determination of Acidity in Ice Cores". In: *Environmental Science & Technology* 50.19, pp. 10485–10493. ISSN: 0013-936X. DOI: 10.1021/acs.est.6b00026. URL: https://doi.org/10.1021/acs.est.6b00026.

Kreutz, K. J. and B. G. Koffman (2013). *Glaciochemistry*. DOI: 10.1016/B978-0-444-53643-3.00312-5.

Langway Jr., C. C. (2008). *The History of Early Polar Ice Cores*. Tech. rep. January. US Army Corps of Engineers Engineer Research and Development Center, p. 47.

Legrand, M. and P. Mayewski (1997). "Glaciochemistry of polar ice cores: A review". In: *Reviews of Geophysics* 35.3, pp. 219–243. ISSN: 87551209. DOI: 10.1029/96RG03527.

Legrand, M. et al. (2016). "Boreal fire records in Northern Hemisphere ice cores: A review". In: *Climate of the Past* 12.10, pp. 2033–2059. ISSN: 18149332. DOI: 10.5194/cp-12-2033-2016.

Mahowald, N. et al. (1999). "Dust sources and deposition during the last glacial maximum and current climate: A comparison of model results with paleodata

from ice cores and marine sediments". In: *Journal of Geophysical Research Atmospheres* 104.D13, pp. 15895–15916. ISSN: 01480227. DOI: 10.1029/1999JD900084.

Mortensen, A. et al. (2005). "Volcanic ash layers from the last glacial termination in the NGRIP ice core". In: *Journal of Quaternary Science* 20.3, pp. 209–219. ISSN: 02678179. DOI: 10.1002/jqs.908.

Neftel, A. et al. (Jan. 1985). *Measurements of a Kind of DC-Conductivity on Cores from Dye 3*. DOI: doi:10.1029/GM033p0032. URL: https://doi.org/10.1029/GM033p0032.

Rasmussen, S. O. et al. (2007). "Early Holocene climate oscillations recorded in three Greenland ice cores". In: *Quaternary Science Reviews* 26.15-16, pp. 1907–1914. ISSN: 02773791. DOI: 10.1016/j.quascirev.2007.06.015.

Rasmussen, S. O. et al. (2013). "A first chronology for the North Greenland Eemian Ice Drilling (NEEM) ice core". In: *Climate of the Past* 9.6, pp. 2713–2730. DOI: 10.5194/cp-9-2713-2013. URL: https://www.clim-past.net/9/2713/2013/.

Rasmussen, S. O. et al. (2014). "A stratigraphic framework for abrupt climatic changes during the Last Glacial period based on three synchronized Greenland ice-core records: Refining and extending the INTIMATE event stratigraphy". In: *Quaternary Science Reviews* 106, pp. 14–28. ISSN: 02773791. DOI: 10.1016/j.quascirev.2014.09.007. URL: http://dx.doi.org/10.1016/j.quascirev.2014.09.007.

Reeh, N., S J Johnsen, and D Dahl-Jensen (Jan. 1985). *Dating the Dye 3 Deep Ice Core by Flow Model Calculations*. DOI: doi:10.1029/GM033p0057. URL: https://doi.org/10.1029/GM033p0057.

Röthlisberger, R. et al. (2000). "Technique for continuous high-resolution analysis of trace substances in firn and ice cores". In: *Environmental Science and Technology* 34.2, pp. 338–342. ISSN: 0013936X. DOI: 10.1021/es9907055.

Ruth, U. et al. (2003). "Continuous record of microparticle concentration and size distribution in the central Greenland NGRIP ice core during the last glacial period". In: *Journal of Geophysical Research: Atmospheres* 108.3, pp. 1–12. ISSN: 01480227. DOI: 10.1029/2002jd002376.

Schüpbach, S. et al. (2018). "Greenland records of aerosol source and atmospheric lifetime changes from the Eemian to the Holocene". In: *Nature Communications* 9.1. ISSN: 20411723. DOI: 10.1038/s41467-018-03924-3. URL: http://dx.doi.org/10.1038/s41467-018-03924-3.

Shepherd, A. et al. (2020). "Mass balance of the Greenland Ice Sheet from 1992 to 2018". In: *Nature* 579.7798, pp. 233–239. ISSN: 14764687. DOI: 10.1038/s41586-019-1855-2.

Shoji, H. and C. C. Langway Jr. (Jan. 1985). *Mechanical Properties of Fresh Ice Core from Dye 3, Greenland*. DOI: doi:10.1029/GM033p0039. URL: https://doi.org/10.1029/GM033p0039.

Sigg, A. et al. (Feb. 1994). "A continuous analysis technique for trace species in ice cores". In: *Environmental Science & Technology* 28.2, pp. 204–209. ISSN: 0013-936X. DOI: 10.1021/es00051a004. URL: https://doi.org/10.1021/es00051a004.

Simonsen, M. et al. (2018). "Particle shape accounts for instrumental discrepancy in ice core dust size distributions". In: *Climate of the Past* 14.5, pp. 601–608. ISSN: 18149332. DOI: 10.5194/cp-14-601-2018.

Simonsen, M. et al. (2019). "East Greenland ice core dust record reveals timing of Greenland ice sheet advance and retreat". In: *Nature Communications* 10.1. ISSN: 20411723. DOI: 10.1038/s41467-019-12546-2. URL: http://dx.doi.org/10.1038/s41467-019-12546-2.

Stauffer, B. et al. (Jan. 1985). *CO2 Concentration in Air Extracted from Greenland Ice Samples*. DOI: doi:10.1029/GM033p0085. URL: https://doi.org/10.1029/GM033p0085.

Steffensen, J.P. (1995). "Microparticles and chemial impurities in ice cores from Dye 3, South Greenland and their interpretation in palaeoclimatic reconstructions". PhD thesis. University of Copenhagen, p. 106.

— (1997). "The size distribution of microparticles from selected segments of the Greenland Ice Core Project ice core representing different climatic periods". In: *Journal of Geophysical Research* 102.C12, pp. 755–26. ISSN: 0148-0227.

Svensson, A. (2014). *Ice Cores*. DOI: 10.1007/978-94-007-6326-5.

Svensson, A. et al. (2020). "Bipolar volcanic synchronization of abrupt climate change in Greenland and Antarctic ice cores during the last glacial period". In: *Climate of the Past Discussions* 2020, pp. 1–28. DOI: 10.5194/cp-2020-41. URL: https://www.clim-past-discuss.net/cp-2020-41/.

Venkatesh, J. (2020). *An improved Gas-CFA system for methane measurements and preliminary results from the Dye-3 ice core, M.Sc. Thesis*. Copenhagen, Denmark.

Vinther, B. M. et al. (2006). "A synchronized dating of three Greenland ice cores throughout the Holocene". In: *Journal of Geophysical Research Atmospheres* 111.13, pp. 1–11. ISSN: 01480227. DOI: 10.1029/2005JD006921.

Yau, A. et al. (2016). "Setting a chronology for the basal ice at Dye-3 and GRIP: Implications for the long-term stability of the Greenland Ice Sheet". In: *Earth and Planetary Science Letters* 451, pp. 1–9. ISSN: 0012-821X. DOI: https://doi.org/10.1016/j.epsl.2016.06.053. URL: http://www.sciencedirect.com/science/article/pii/S0012821X16303405.

Image on title page:

Angela Blumen (2019), *Untitled* (photograph). Used with permission.

Appendix

A. Freezer cutting log

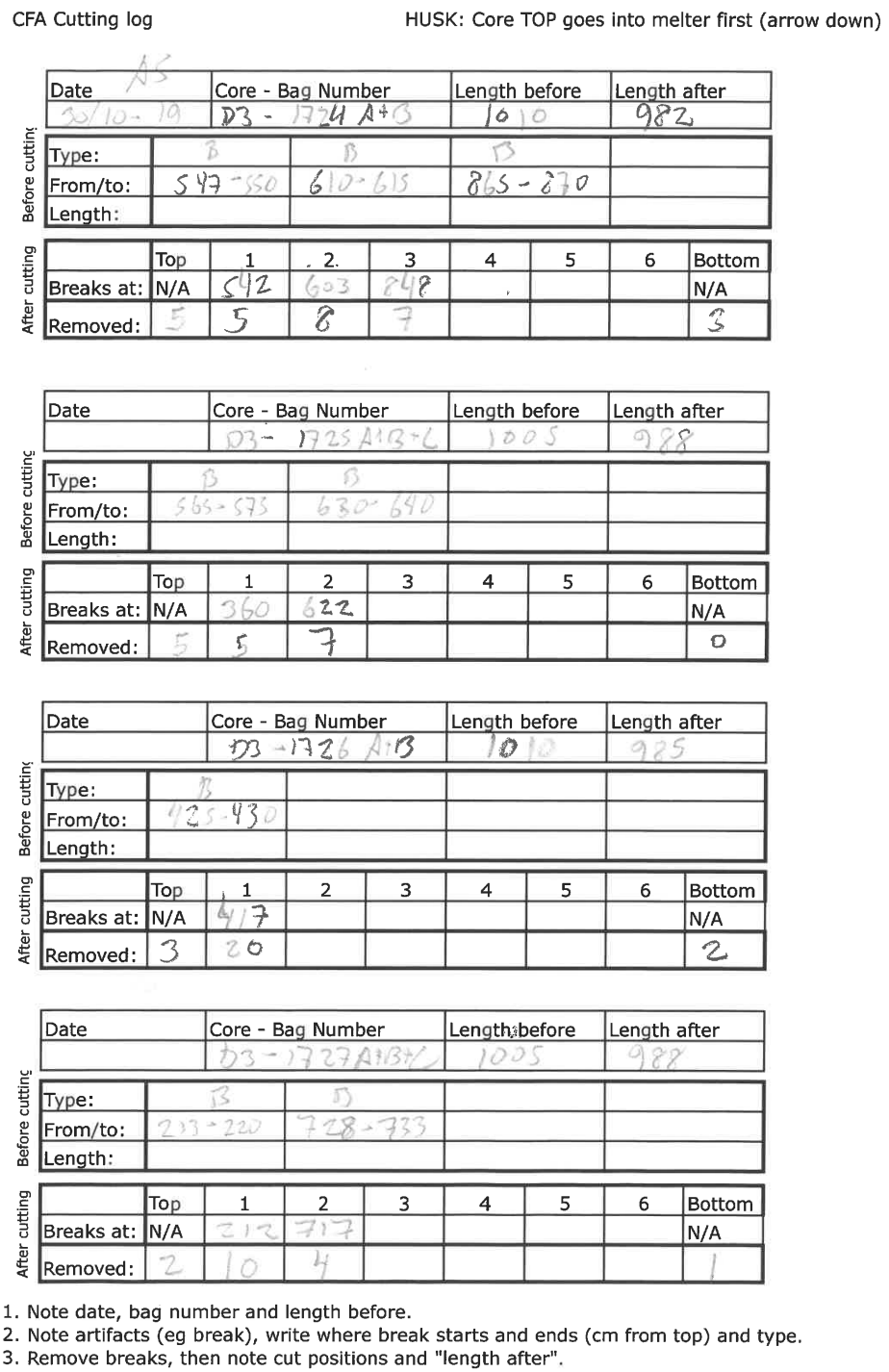

CFA Cutting log — HUSK: Core TOP goes into melter first (arrow down)

Date	Core - Bag Number	Length before	Length after
25/10-19	D3 - 1724 A+B	1010	982

Before cutting

Type:	B	B	B
From/to:	547-550	610-615	865-870
Length:			

After cutting

	Top	1	2	3	4	5	6	Bottom
Breaks at:	N/A	542	603	848				N/A
Removed:	5	5	8	7				3

Date	Core - Bag Number	Length before	Length after
	D3- 1725 A+B+C	1005	988

Before cutting

Type:	B	B	
From/to:	565-573	630-640	
Length:			

After cutting

	Top	1	2	3	4	5	6	Bottom
Breaks at:	N/A	360	622					N/A
Removed:	5	5	7					0

Date	Core - Bag Number	Length before	Length after
	D3 -1726 A+B	1010	925

Before cutting

Type:	B		
From/to:	425-430		
Length:			

After cutting

	Top	1	2	3	4	5	6	Bottom
Breaks at:	N/A	417						N/A
Removed:	3	20						2

Date	Core - Bag Number	Length before	Length after
	D3 - 1727 A+B+C	1005	988

Before cutting

Type:	B	B	
From/to:	213-220	728-733	
Length:			

After cutting

	Top	1	2	3	4	5	6	Bottom
Breaks at:	N/A	212	717					N/A
Removed:	2	10	4					1

1. Note date, bag number and length before.
2. Note artifacts (eg break), write where break starts and ends (cm from top) and type.
3. Remove breaks, then note cut positions and "length after".

Figure A. Example page from the cutting log used to record the removal of ice at each break.

B. Diagram of CFA setup for gas extraction and analysis

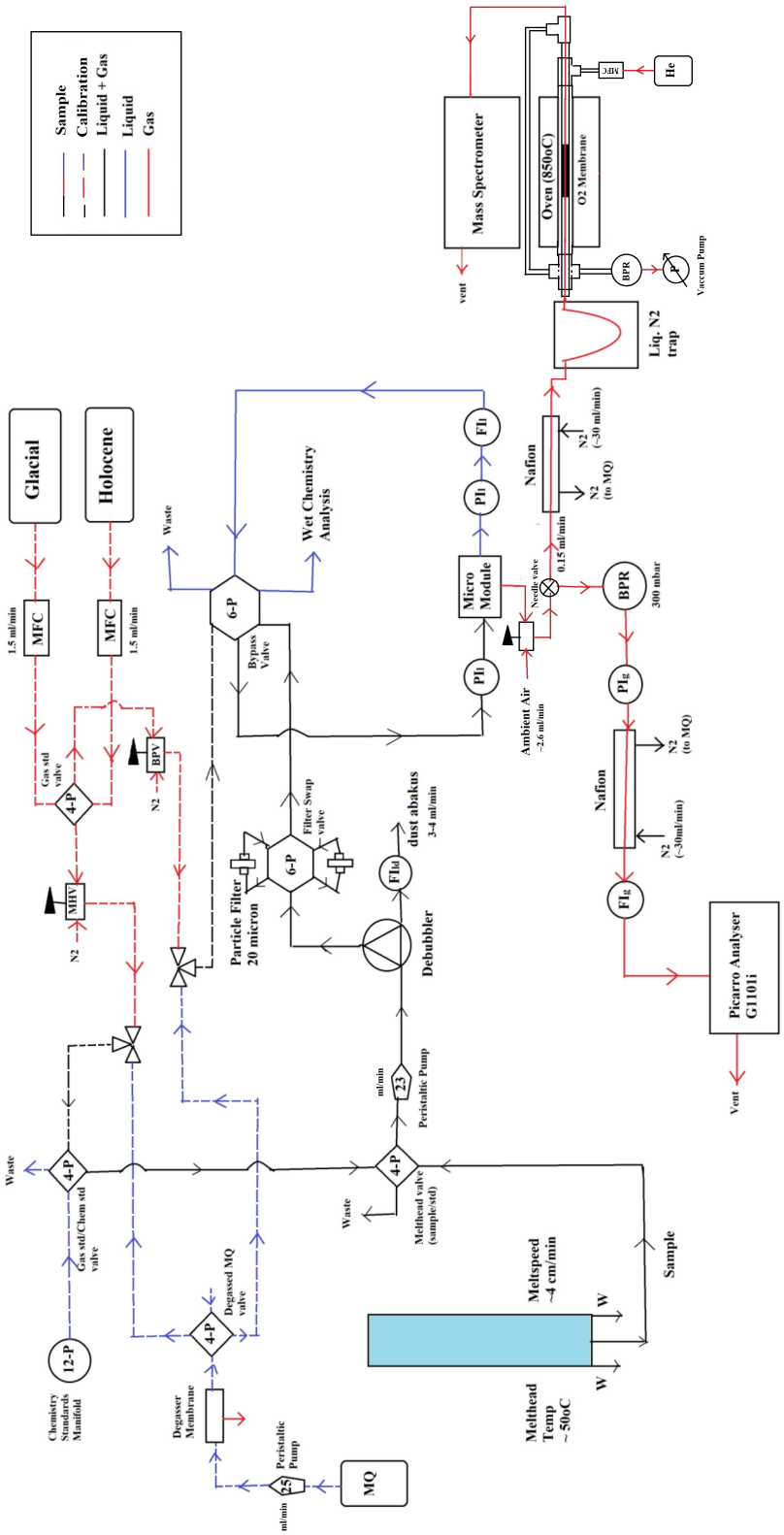

Figure B. CFA system diagram including gas extraction and analysis setup (Figure courtesy of Janani Venkatesh, reproduced from Venkatesh (2020))

C. Age scale match points

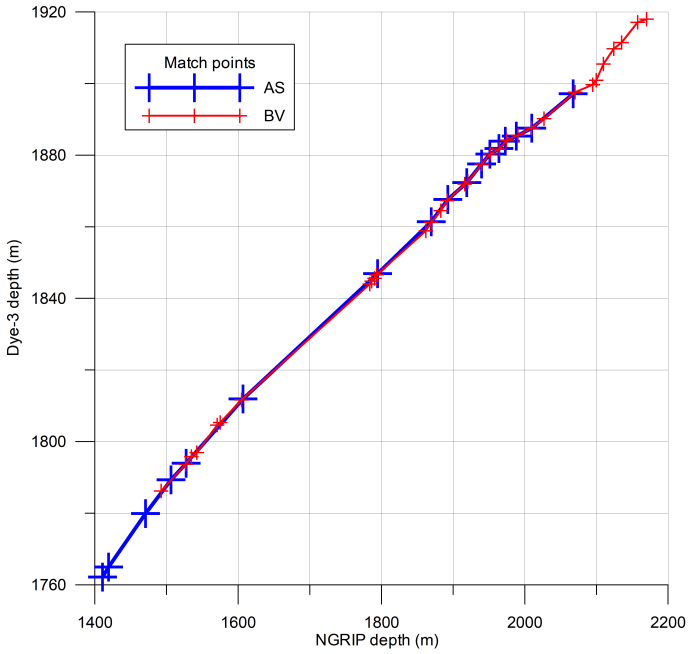

Figure C. Match points used in the creation of the updated preliminary Dye 3 age scale. AS = match points added by Anders Svensson, BV = match points added by Bo Vinther. Figure courtesy of Anders Svensson (personal correspondence).

D. Standard calibrations and delay times

	Delay times (seconds)					Standard calibration slope (*alpha*)				Baseline (I_0)		
Run	Cond.	Dust	pH	Ca^{2+}	NH_4^+	Ca^{2+}	NH_4^+	pH (acid)	pH (alkaline)	Ca^{2+}	NH_4^+	pH
1704	32	32	88	112	139	215.6909	1893.9	0.0034	0.0053	56176	9789.16667	40880
1712	38	38	94	119	145	199.3765	1713.8	0.0032	0.0047	60075	10077.3973	41857
1720	40	40	97	122	146	211.4082	1917.1	0.0034	0.0051	57177	8118.82344	41739
1730	30	30	91	109	136	240.601	1754	0.0032	0.0047	35026	8926.53684	41416
1738	38	38	90	118	145	254.3762	1862.5	0.0036	0.0047	33387	8732.014	41432
1752	35	35	86	114	139	227.7402	1713.1	0.0035	0.0055	42268	7921.03014	36078
1816	40	40	91	120	145	284.0918	1567.6	0.0039	0.0045	42239	7669.78947	34513
1825	45	45	104	125	150	223.1268	1877.2	0.0017	0.0044	38590	6662.24277	51104
1828	40	40	99	120	145	223.1268	1877.2	0.0017	0.0044	40784	6662.24277	50351
1831	37	37	105	117	143	250.513	1878.5	0.002	0.0044	38220	8249.611	49622
1834	35	35	103	115	141	250.513	1878.5	0.002	0.0044	37631	8249.611	49789
1843	41	41	88	121	145	227.3558	1829.7	0.0006	0.0007	38138	6576.23261	58832
1853	29	29	150	111	135	235.1902	1854.4	0.0029	0.0041	34604	5381.08517	22393
1862	42	42	96	122	145	230.379	1836.9	0.0033	0.0036	34263	6270.01849	46711
1865	42	42	94	125	147	222.558	1905.6	0.0026	0.004	33112	9416.72878	46132

Figure D. Delay times and standard calibration values (courtesy of Aylin De Campo) used for each run.